

Review

Lunar and Martian Silica

Masahiro Kayama ^{1,2,*} , Hiroshi Nagaoka ^{3,4}  and Takafumi Niihara ^{5,6} 

¹ Creative Interdisciplinary Research Division, Frontier Research Institute for Interdisciplinary Sciences, Tohoku University, Sendai 980-8578, Japan

² Department of Earth and Planetary Materials Science, Graduate School of Science, Tohoku University, Sendai 980-8578, Japan

³ Research Institute for Science and Engineering, Waseda University, Tokyo 169-8555, Japan; hiroshi-nagaoka@asagi.waseda.jp

⁴ Institute of Space and Astronautical Science, Japan Aerospace Exploration Agency, Sagamihara 252-5210, Japan

⁵ Department of Systems Innovation, University of Tokyo, Tokyo 113-8656, Japan; niihara@sys.t.u-tokyo.ac.jp

⁶ University Museum, University of Tokyo, Tokyo 113-0033, Japan

* Correspondence: masahiro.kayama.a3@tohoku.ac.jp; Tel.: +81-22-795-6687

Received: 1 May 2018; Accepted: 14 June 2018; Published: 25 June 2018



Abstract: Silica polymorphs, such as quartz, tridymite, cristobalite, coesite, stishovite, seifertite, baddeleyite-type SiO₂, high-pressure silica glass, moganite, and opal, have been found in lunar and/or martian rocks by macro-microanalyses of the samples and remote-sensing observations on the celestial bodies. Because each silica polymorph is stable or metastable at different pressure and temperature conditions, its appearance is variable depending on the occurrence of the lunar and martian rocks. In other words, types of silica polymorphs provide valuable information on the igneous process (e.g., crystallization temperature and cooling rate), shock metamorphism (e.g., shock pressure and temperature), and hydrothermal fluid activity (e.g., pH and water content), implying their importance in planetary science. Therefore, this article focused on reviewing and summarizing the representative and important investigations of lunar and martian silica from the viewpoints of its discovery from lunar and martian materials, the formation processes, the implications for planetary science, and the future prospects in the field of “micro-mineralogy”.

Keywords: silica; moon; Mars; lunar and martian meteorites; Apollo samples; remote-sensing observation; igneous process; shock metamorphism; hydrothermal fluid activity

1. Introduction

Silica is one of the constituent minerals in the Earth’s crustal rocks, and is one of the minor minerals that is often distributed in extraterrestrial materials such as lunar and martian meteorites, returned samples (Apollo and Luna collections), and the parent bodies (e.g., the Moon and Mars). Over the past ten years, various types of silica polymorphs (e.g., quartz, tridymite, cristobalite, moganite, coesite, stishovite, seifertite, and baddeleyite-type SiO₂) and non-crystalline silica (high-pressure (HP) silica glass and opal) have been reported in lunar and martian rocks using microanalyses and studying the celestial bodies through remote-sensing observations (Table 1), although a lack of the diversity and wide distribution was believed before. For example, several previous investigations have supported the hypothesis that few high-pressure phases are included in lunar meteorites, despite the existence of many craters and regoliths, because a part of them (e.g., the high-pressure SiO₂ phases) may be volatilized during impact collisions under the high vacuum condition of the Moon [1,2]. However, recent studies have revealed that coesite, stishovite, and seifertite lie in several lunar meteorites and an Apollo collection [3–5]. Hydrothermal silica was believed to be absent from

extraterrestrial materials, but moganite and opal-A, originating from the fluid activity of the parent bodies, have recently been discovered from lunar and martian meteorites [6,7]. Opaline silica deposits have also been observed in association with martian volcanic materials by the Mars rover “Spirit and Opportunity” [8]. In addition, silica nanoparticles were detected in Enceladus by the Cassini spacecraft [9,10]. Of course, for decades, many researchers have reported igneous silica such as quartz, tridymite, and cristobalite in various types of extraterrestrial materials, especially in lunar samples (lunar meteorites and Apollo and Luna collections) and martian meteorites [11,12]. From the latest viewpoint of planetary science, there seems to be a wide variety of silica polymorphs in the solar system.

According to the pressure–temperature phase diagram for SiO₂ (Figure 1) (e.g., [13–17]), quartz, tridymite, and cristobalite, as well as coesite and stishovite, are stable at different pressure and temperature regions. The high-temperature and high-pressure SiO₂ phases are quenchable down to ambient conditions, and thus exist in extraterrestrial materials via rapid cooling processes during magmatic eruption, decompression after impact events, or aqueous fluid activity. For example, seifertite is thermodynamically stable at more than ~100 GPa, which is not realistic for an impact event on the Moon and Mars. However, seifertite can be converted as a metastable phase from cristobalite at ~11 GPa, and can consequently be quenched down to an ambient condition [18]. As a result of this process, seifertite remains present in some of the lunar and martian meteorites that have experienced the host bodies [4,18,19]. Thus, the occurrence of these high-temperature and high-pressure SiO₂ phases allows us to set constraints for the crystallization temperature, cooling rate, and shock pressure and temperature, which provide valuable information on magma eruption (e.g., [12,20]) and the sizes of the crater and impactor that collided on the parent bodies (e.g., [4,21]). In addition, the metastable SiO₂ phase moganite has been found to be distributed in a lunar meteorite, which is thought to have precipitated from high-pressure alkaline fluid activity on the Moon [7]. Based on the moganite precipitation model, the bulk content of H₂O ice in the Moon’s subsurface can be theoretically calculated. Thus, igneous, shock metamorphic, and hydrothermal events of various celestial bodies have been interpreted by a mineralogical description of such extraterrestrial silica.

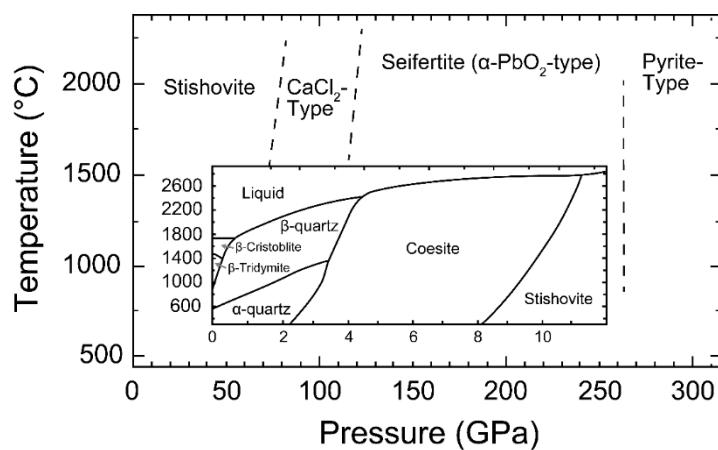


Figure 1. Phase diagram of SiO₂ modified after [15–17]. Metastable SiO₂ phases of moganite, HP-glass, and likely baddeleyite-type SiO₂ are not described here.

Table 1. Silica polymorphs discovered from lunar samples and martian meteorites.

Name	Crystal System	Space Group	Lattice Parameter (Å)				Density (g/cm ³)	Occurrence	Reference
			a	B	c	β			
α-Quartz	Trigonal	<i>P3₁21</i> or <i>P3₂21</i>	4.9137	4.9137	5.4047	90	2.6486	Lunar/martian samples	[22]
α-Tridymite	Monoclinic	<i>Cc</i> or <i>C2/c</i>	18.52	4.98	23.79	105.6	2.27	Lunar samples	[23]
	Triclinic (pseudo-orthorhombic)	<i>F1</i>	9.932	17.216	81.864	90	2.281	Terrestrial rocks *	[24]
α-Cristobalite	Tetragonal	<i>P4₁2₁2</i>	5.063	5.063	6.99	90	2.227	Lunar/martian samples	[4]
Coesite	Monoclinic	<i>C2/c</i>	7.14	12.45	7.17	120.02	2.89	Lunar/martian meteorites	[7]
Stishovite	Tetragonal	<i>P4₂/mmm</i>	4.204	4.204	2.678	90	4.216	Lunar/martian samples	[4]
Seifertite	Orthorhombic	<i>Pbcn</i> or <i>Pnc2</i>	4.097	5.0462	4.4946	90	4.2949	Lunar/martian meteorites	[25]
Baddeleyite-type	Monoclinic	<i>P21/c</i>	4.375	4.584	4.708	99.97	4.3	Martian meteorite	[26]
α-Moganite	Monoclinic	<i>I2/a</i>	8.77	4.90	10.77	90.38	2.59	Lunar meteorite	[7]
Opal-A	-	-	-	-	-	-	-	Martian meteorite	[6]

* Triclinic α-Tridymite has only been reported in terrestrial samples, but a monoclinic one has been invariably discovered from extraterrestrial materials.

Among the extraterrestrial materials, the Apollo and Luna collections, and lunar and martian meteorites, contain relatively abundant silica, reaching the bulk content of a few weight percentage at most. Some of the silica occurs as millimeter-sized to a few ten micrometer-sized euhedral or subhedral crystals, most of which have been identified as igneous tridymite and cristobalite (e.g., [27]). The coarse silica crystals affected by heavy impact events (high shock pressure-induced asteroidal collisions) frequently possess tweed or lamellae textures in their rim, where coesite, stishovite, and seifertite nanoparticles are present [4,5,19,26]. The other silica exists as subhedral to anhedral fine grains with a size of micrometers to submicrometers. In some cases, such fine silica grains appear as single crystals of igneous quartz, tridymite, and cristobalite, or consist of a mixture of numerous silica nanoparticles (quartz, cristobalite, coesite, stishovite, seifertite, and HP silica glass) because of impact events on the extraterrestrial materials. Recent investigations have also demonstrated the presence of microcrystalline aggregates of moganite with other silica polymorphs [7], as well as single nanoparticles of opal-A [6], in lunar and martian meteorites, respectively, both of which may have precipitated from hydrous fluid in the parent bodies. As described above, such micro-mineralogy of extraterrestrial silica is an important subject with regards to the implications for planetary science. However, some reports of extraterrestrial materials have only mentioned silica based on observations under optical microscope or scanning electron microscope (SEM), and did not determine the type of silica polymorphs, especially for the fine silica grains, using advanced microanalysis such as Raman microscopy, synchrotron angle dispersive X-ray diffraction (SR-XRD), transmission electron microscopy (TEM), and electron back scatter diffraction (EBSD).

Here, the purpose of this paper was to review and summarize representative and important micro-mineralogical studies of various silica polymorphs in the lunar and martian materials that have been reported up until now. Additionally, several case studies of silica that have been observed in celestial bodies by remote-sensing spacecraft have been included. In each category, named “Moon” and “Mars”, we describe the types of SiO₂ phase, their occurrence, and the implications for planetary science, as well as the implied future prospects in the field of micro-mineralogy. Subsections within these categories address the origin of silica in the parent bodies.

2. Moon

2.1. Lunar Igneous Process

The Moon is a celestial body that has experienced differentiation from a lunar magma ocean (LMO) to its crust and mantle [28]. When we view the Moon from the Earth, the Moon is roughly divided into two regions, called terranes (Figure 2a,b). Bright and white-colored terranes are called “highland”, and are thought to be a relic of an initial feldspathic crust solidified from a LMO. The feldspathic crust was formed by the flotation of light plagioclase due to the difference in densities between plagioclase and melt in the LMO. In contrast, heavy minerals, such as olivine and pyroxene, sank after crystallization and accumulated as a massive mafic mantle. Dark and black-colored terranes are known as maria, which are composed of basaltic magma originating from repeated partial melting and eruptions of the mafic mantle. Considering crater counts on the lunar surface (e.g., [29,30]), the basaltic igneous activities after the initial crust formation continued on the Moon for a long period of time (by 1–2 Ga). More concrete evidence of extended lunar igneous activity is evidenced by radiometric dating of lunar meteorites. The youngest sample of mare basalt dated so far, Northwest Africa 032, yielded a Rb–Sr age of 2947 ± 16 Ma [31]. Furthermore, the lunar surface can be geochemically divided into three major terranes (except for the maria) from the global standpoint of the Moon: the Feldspathic Highland Terrane (FHT), with low-Fe and low-Th contents; the Procellarum KREEP (high potassium, rare earth element, and phosphorus) Terrane (PKT), with medium-Fe and high-Th contents; and the South-Pole Aitken (SPA) terrane [32]. The FHT corresponds to the highland; the PKT is a terrane surrounding the Mare Imbrium and Oceanus Procellarum; and the SPA terrane is located on the farside of the moon, and is the largest impact basin on the Moon (Figure 2c,d). Details of each geochemical feature can be found in Jolliff et al. [32].

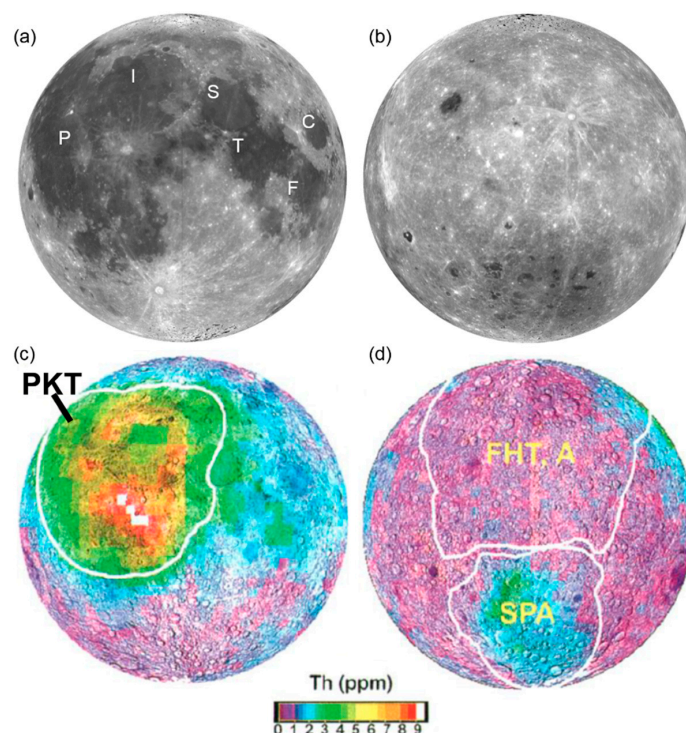


Figure 2. Albedo map of the Moon: (a) the nearside (face to earth), (b) the farside obtained by SELENE mission [33]. Label C points to the Mare Crisium, Label F points to the Mare Fecunditatis, Label T points to the Mare Tranquilitatis, Label S points to the Mare Serenitatis, Label I points to the Mare Imbrium, and Label P points to the Oceanus Procellarum. Th map of the Moon: (c) the nearside, (d) the farside [32]. PKT = Procellarum KREEP Terrane; FHT, A = Feldspathic Highland Terrane, Anorthositic; and SPA = South-Pole Aitken.

Silicate minerals are the most abundant minerals on the lunar surface, most of which belong to olivine ($(\text{Mg,Fe})_2\text{SiO}_4$), pyroxene ($(\text{Mg,Fe})_2\text{Si}_2\text{O}_6$ – $(\text{Ca,Mg,Fe})_2\text{Si}_2\text{O}_6$), and plagioclase ($\text{CaAl}_2\text{Si}_2\text{O}_8$ – $\text{NaAlSi}_3\text{O}_8$) groups. Plagioclase has a low albite component, and K-feldspar (KAlSi_3O_8) is apparently a minor mineral on the Moon when compared with the Earth. Some locations with high abundances of specific minerals have been reported as endmembers of LMO: purest anorthosite (>98 vol % plagioclase) and olivine exposures with a dunite composition based on global remote-sensing data [34,35]. Oxide minerals are the second most abundant rock constituents. Among them, ilmenite (FeTiO_3) occurs most frequently on the Moon. It is commonly distributed in mare basalt, and its abundance varies largely from place to place [36,37]. Silica (SiO_2) is generally rare in lunar materials when compared with lunar silicate and ilmenite, as mentioned above. Phosphate minerals also occur as minor minerals in lunar rocks.

Silica found in lunar samples can be traced to three origins: igneous processes, shock metamorphism due to impact events, and hydrothermal fluid activity. The first origin leads to silica polymorphs of cristobalite, tridymite, and quartz; the second to coesite, stishovite, seifertite, baddeleyite-type SiO_2 , and HP silica glass; and the third to moganite (Table 1). The mineralogy and petrology of shock-induced and aqueous silica polymorphs on the Moon are discussed in Sections 2.2 and 2.3, and lunar igneous silica is reviewed in light of recent studies of the Apollo collections, lunar meteorites, and remote-sensing observations.

2.1.1. Apollo Collections

The Apollo and Luna missions returned several kinds of samples from a total of nine locations distributed on the near side of the Moon from the 1960s to 1970s (Table 2). The total weight of all

the returned samples was up to 382 kg. Six times, the Apollo astronauts collected rocks, regolith, soil, volcanic glass beads, and drill core samples. The Luna missions obtained regolith samples by drill core sampling automatically on three occasions. The locations and lithologies of the Apollo and Lunar collections are summarized as follows: the Apollo 11 and 12 and Luna 16 and 24 missions returned the mare basaltic samples. The Apollo 16 and Luna 20 missions obtained feldspathic samples from the highlands. The Apollo 15 and 17 missions set down and collected samples from the highland/mare boundary. The Apollo 14 mission landed in a geological and geochemical anomalous region, the PKT, of which the returned samples were highly enriched in incompatible elements such as rare earth elements (REE), potassium (K), and Th. Most of the Apollo-returned regolith samples were brecciated by impact events and were mixed with KREEP materials, which are enriched in elements such as potassium (K), rare earth elements (REE), and phosphorus (P) [2], because the Apollo landing sites were located around geochemically anomalous regions restricted in the central nearside of the Moon near the PKT. The geochemical anomaly of the Apollo 14 landing site was revealed later, where the Th abundances were highly enriched within PKT, as determined by a spacecraft mission by the Lunar prospector gamma-ray spectrometer [32].

Table 2. Summary of landing sites, returned sample weight, and returned date of the Apollo and Luna missions [38].

Mission	Landing Site	Sample Weight (kg)	Returned Date
Apollo 11	Mare Tranquilitatis	21.6	24 July 1969
Apollo 12	Oceanus Procellarum	34.3	24 November 1969
Apollo 14	Mare Imbrium	42.3	9 February 1971
Apollo 15	Hadley Rille/Appenine Mts	77.3	7 August 1971
Apollo 16	Descartes Highlands	95.7	27 April 1972
Apollo 17	Mare Serenitatis	110.5	19 December 1972
Luna 16	Mare Fecunditatis	0.10	24 September 1970
Luna 20	Apollonius Highlands	0.03	25 February 1972
Luna 24	Mare Crisium	0.17	22 August 1976

Igneous silica was mostly found in the Apollo collections in the following rock types: mare basalt, quartz monzodiorite (QMD), granite, and felsite (fine-grained granite). Cristobalite is the most common silica in lunar basalts [2]. These lithological characteristics of lunar basalts are different from those of terrestrial basalts, which do not contain silica as a free phase. The Apollo sample, 15405 possesses several types of lithic fragments, such as coarse-grained granite, KREEP-rich QMD, and basalt with high-KREEP compositions (KREEP basalt), as described in [39]. Silica occurs in the granite as large, crushed, and discrete fragments, sometimes displaying grains with a characteristic fractured texture or fine-grained intergrowths with K-feldspar. This fractured textural pattern of the silica corresponds to a habit of cristobalite. QMD contains more ilmenite and phosphate, and less silica (5 or 10%), represented by assumed cristobalite, as in the case of the granite. Silica occurs in QMD in two different microtextural contexts (i.e., in the intergrowths with K-feldspar and/or as individual single grains), the same as in the granite [39]. Jolliff [11] described a SiO₂ phase in Apollo 14 QMD (14161,7069) occurring as single grains (up to 300 µm) being fractured into a mosaic pattern similar to the texture in 15405 granite [39]. However, this mineralogical description of possible cristobalite is only based on morphology and texture and no direct phase analysis [39].

Quartz is generally present in the granitic (or felsic) samples of the Apollo 12, Apollo 14, and Apollo 17 landing sites. These granitic rocks are rich in incompatible trace elements (ITE) and only comprise <0.03% of the mass of all Apollo samples [40]. Lunar granite is different from terrestrial ones because of the absence of mica and amphibole. Mineralogical and petrological investigations of silica in the Apollo samples up until a decade ago were reviewed by [2,27,37]. Therefore, this article focused on recent works on silica polymorphs in the Apollo samples.

A recent study of the Apollo 12 samples [41] reported a quartz-bearing granite fragment (12023,147-10), which possessed two different textures: (1) 80 vol % granophyric intergrowths of

K-feldspar and quartz, and (2) 15 vol % intergrowths (or mirmekitic texture) of plagioclase and quartz. Quartz within the former intergrowths was present as an inter-connected fretwork of elongate crystals typically 100 μm in length and 1–15 μm in width, or quartz laths within the K-feldspar grains. The latter was an anhedral, frequently curved quartz intergrown with K-feldspar or plagioclase. The remaining 5 vol % of this granite consisted of hedenbergitic pyroxene, fayalitic olivine, and ilmenite with other trace minerals such as zircon, yttrite, thorite, apatite, Fe-metal, and monazite. The silica was identified as quartz by Raman spectroscopy. The crystallization age of this granite is 3.87 ± 0.03 Ga, using Th–U–Pb geochronology derived from an electron microprobe analyzer (EMPA) of thorite, which is relatively young among the lunar granites. The U/Pb method for zircon in lunar granophyre provides two different crystallization ages: (1) as old as 4.3 Ga, and (2) as young as 3.9 Ga. The older group was derived from the residue liquid of the LMO [42]. In contrast, the relatively young crystallization age of the Apollo 12 granite fragment (12023,147-10) suggested that the granite was related to the formation of the Imbrium impact basin where it was formed by heating and melting [41]. Seddio et al. [40] investigated other granitic fragments in the returned Apollo 12 samples: 12001,909-14, 12032,367-16, 12033,634-30, and 12033,634-34. Sample 12001,909-14 was a complex polymict granitic breccia, where the breccia phases were categorized in seven areas based on different textures and mineral compositions. Furthermore, the modal abundances of silica in the breccia phases were 4.5–37% among the seven areas. The other samples each included ~20 vol % silica. Quartz is the most common silica polymorph in lunar granite. A hackle fracture pattern of the quartz was caused by an inversion from the high-temperature and low-pressure silica polymorph of tridymite or cristobalite.

2.1.2. Lunar Meteorites

Lunar meteorites came to the Earth from the Moon by launching from the lunar surface via meteoroid or asteroid collisions. In other words, the Apollo and Luna missions only collected samples from a relatively small and geochemically anomalous region of the lunar nearside, but lunar meteorites come randomly from the entire Moon [43]. The launch processes of lunar meteorites provide global information on lunar geochemical and petrological features (e.g., [44–52]). The total estimated numbers show that 139 paired meteorites have been recovered on Earth [53]. Among them, most of the igneous silica polymorphs have been found in the basaltic or granitic clasts in lunar meteorites, similar to the Apollo returned samples.

Some of the silica-bearing igneous clasts have been recognized in the lunar meteorite, Northwest Africa (NWA) 773 clan, which is a series of paired lunar meteorites of NWA 773, NWA 2727, NWA 2977, NWA 6950, and others. Most are basaltic breccias containing igneous clasts of various lithologies including olivine gabbro, olivine phyric basalt, pyroxene phyric basalt, pyroxene gabbro, ferroan symplectite, and alkali-rich-phase ferroan rocks (ARFe) [54–56]. In fact, NWA 2977 and NWA 6950 consist entirely of olivine gabbro. Small angular fragments (<100–200 μm) of silica glass also occur in the breccia, which have two possible origins: (1) a transition of the crystalline phase to silica glass by shock metamorphism, or (2) an original amorphous phase [55]. Silica is included in ferroan symplectite, ARFe clasts, and clasts of a late-stage assemblage of silica–K–feldspar–plagioclase intergrowths plus troilite, baddeleyite, and REE-bearing-merrillite [54–56]. The symplectite clasts consist of fine-grained curved intergrowths of fayalite, hedenbergitic pyroxene, and silica [54,56]. It is difficult to determine whether the symplectitic silica is crystalline or amorphous because of its fine-grained size [55]. Fagan et al. [56] suggested that the silica was formed by the breakdown of pyroxferroite on the basis of the mineral assemblage. The alkaline-phase-ferroan clasts are composed of fayalitic olivine, hedenbergitic pyroxene, silica, and Ca–phosphates. Silica occurs as elongate crystals or K-rich glass + silica. Their mineral assemblage and ferroan compositions are similar to those of the symplectite clasts, but their textural morphologies are different to those of the ARFe clasts [56]. Fagan et al. [56] implied a petrological connection between a basaltic magma system to form the olivine gabbro and a silicic magma system to generate the symplectite and ARFe clasts. The crystallization ages of the olivine gabbro lithology are much younger (3.0–3.1 Ga [31,57]) than those of the Apollo

granophyric samples (3.9–4.3 Ga). On the Moon, complex igneous activities that produce silica-rich magma could have possibly continued longer than the Apollo granophyric samples suggest.

Cristobalite is a minor mineral, based on Raman spectroscopic measurements of a basaltic lunar meteorite, LaPaz Icefield (LAP) 02205, and is a low-Ti mare basalt found in Antarctica [58]. NWA 4734 is a low-Ti basalt, unbrecciated with a medium- to coarse-grained, subophitic texture. NWA 4734 contains 1.5% silica as subhedral to anhedral grains in the mesostasis, where fayalite, ilmenite, and Fe-sulfide coexist, but the crystallographic nature of the silica phase has not been described [59]. Some of the silica crystals in NWA 4734 were converted into high-pressure SiO₂ phases by impact events, as explained in the next section. Sayh al Uhaymir (SaU) 169, a lunar meteorite from Oman, has two different lithologies: the first is a polymict regolith breccia (RB), and the second is an impact-melt breccia (IMB). This lunar meteorite is the most enriched in Th among all lunar meteorites (8.44 ppm Th in RB and 32.7 ppm Th in IMB). A basaltic clast (Basalt 11) in the regolith consists of fayalite, ferroaugite, interstitial silica (tridymite), and ilmenite. The bulk composition indicates an origin from the breakdown of pyroxferroite [60], like in the case of symplectite in NWA 773 [56].

2.1.3. Remote-Sensing Observation

As shown in the above investigations of the returned samples and lunar meteorites, silica is one of the major minerals in the granitic samples. Where did the silicic volcanism that generated igneous silica take place on the Moon? Which magmatic systems formed those rocks? The first question can be answered by global remote-sensing observations. Remote-sensing data can provide us with global information on the Moon, and consequently, possible candidates of silicic volcanism on the lunar surface have already been reported, showing the following characteristics: the Christiansen Feature (CF) observed in the range of the mid-infrared wavelength, high albedo, high Th abundance, and dome-like structures (e.g., [61–65]). The Diviner Lunar Radiometer Experiment onboard the Lunar Reconnaissance Orbiter can detect the signal of silicic volcanism, mineralogically. The three spectral band-pass filters centered at 7.7, 8.25, and 8.55 μm used in the Diviner were designed to characterize silicate mineralogy and the bulk SiO₂ content by the CF. Silicic minerals and lithologies exhibiting short-wavelength positions were observed at several locations: Hansteen Alpha, Lassell, Gruithuisen, and Aristarchus. These are all located within the PKT, where Th is highly concentrated. Outside the PKT, Compton–Belkovich is also an explosive silicic volcanism, where Th abundance is enhanced (14–26 ppm Th) when compared with the surrounding highland [65]. The following three possibilities of magmatic mechanisms are discussed to explain the formation process of silicic magmas on the Moon: differentiation of a mafic magma (or KREEP basalt) [39], magma differentiation with silicate liquid immiscibility [66], and re-melting of the crust because of basaltic underplating [63].

2.2. Shock Metamorphism on the Moon

Since the Apollo era, maskelynite (naturally shock-induced plagioclase glass) and impact melt/glass have been reported in the Apollo collections and lunar meteorites as traces of impact events on the Moon. However, high-pressure minerals have lately been seemingly absent in the lunar samples, although they usually occur in impact craters of the Earth's surface [1,2]. Reasons for this have been discussed. First, high-pressure minerals, especially silica, might be eliminated by impact-induced volatilization under the high vacuum condition on the lunar surface [1,2]. Second, most high-pressure phases in terrestrial impactites, ordinary chondrites, and lunar and martian meteorites are found within and surrounding localized zones of shock melting as veins or pockets, or within amorphous glass (e.g., [17,67,68]). Thus, it seems to have been difficult to determine a structural phase of the nanoparticles using the technique of the time. However, recent investigations of lunar meteorites and an Apollo collection [3–5] have proven the existence of high-pressure minerals such as coesite, stishovite, seifertite, and baddeleyite-type SiO₂ (Table 1) by advanced microanalyses.

High-pressure silica polymorphs of lunar materials have been discovered for the first time from the gabbroic unbrecciated lunar meteorite Asuka-881757 using Raman, TEM, and EBSD

analyses [3]. According to previous studies (e.g., [69,70]), Asuka-881757, found in Antarctica, consists of the constituting minerals of coarse-grained pyroxene (1–2 mm in diameter) and plagioclase (maskelynite) (1–5 mm in diameter), ilmenite with minor chromite, troilite, olivine, apatite, Fe–Ni metal, fayalite–hedenbergite–silica symplectite (at the boundaries between pyroxene and maskelynite), and several grains of silica (50–300 μm in diameter) (Figure 3a). The silica grains are entrained in the shock melt pockets that are composed of mixtures of partially melted, and then quenched, pyroxene and plagioclase glasses. There are many small granular inclusions with a size of 1–10 μm in the silica grains under optical microscope (Figure 3a). Raman spectroscopy demonstrated that most of the silica grains were amorphous because of missing Raman peaks, and the inclusions were coesite (522 cm^{-1}) (Figure 3a) and quartz (464 cm^{-1}). The coesite and quartz inclusions in the silica grains were also identified by EBSD measurements. The crystallographic orientation between the inclusions and the adjacent crystals of coesite is commonly based on the Kikuchi patterns obtained from EBSD data, implying that the inclusions are part of the same skeletal crystal. A similar orientation has been observed between the quartz inclusions and the adjacent quartz. TEM observations of the silica grains showed round-shaped coesite with a size of 300 nm and angular-shaped stishovite with a size of 100 nm.

As a result of these findings, Ohtani et al. [3] interpreted the genesis of the amorphous silica grains containing coesite, stishovite, and quartz to be a result of the transformation of a precursor cristobalite affected by shock metamorphism due to impact. According to a previous study by [1], the silica grains are considered to have originally been cristobalite that was crystallized during the final stage of the host basaltic magma. Because of shock compression during impact events, the cristobalite precursor may have been transformed to stishovite, which constrains the peak pressure to at least 8–30 GPa based on the SiO_2 phase diagram (Figure 1). Considering the angular-shaped morphology, stishovite formed via a solid-state reaction when the shock reached peak pressure. If crystallized from a melt, it should have shown acicular crystals or needles. Furthermore, the silica grains lay in contact with the quenched pyroxene–plagioclase glasses with a clear boundary between them, suggesting that they were not molten during impact events. The Raman spectrum of amorphous portions of the silica grains did not show the characteristic defect band of HP silica glass at about 602 cm^{-1} , where the intensity decreased by annealing at high temperatures, and therefore, the amorphous silica may have been back-transformed from the high-pressure silica polymorphs, such as stishovite, during shock decompression. The preferred crystallographic orientation of coesite and quartz crystals indicated that they were generated in topotactic relation with preexisting crystals such as stishovite. The quartz Raman band is located at 464 cm^{-1} , and did not shift to lower wavenumbers, as in the case of the shocked quartz at 456 cm^{-1} in terrestrial impact craters [71]. In the cases of the Apollo collection 14,163 and 15,271 soils, the main Raman peaks of the quartz shifted to a lower wavenumber and were broadened in width, which may have been caused by a distortion of the SiO_2 framework because of impact events [72]. Therefore, the quartz inclusions seem to have formed because of partial back-transformation from stishovite and/or coesite during decompression. The isotopic ages of Asuka-881757 defined the crystallization age of $3871 \pm 51\text{ Ma}$ by ^{147}Sm – ^{143}Nd dating and the impact age of $3798 \pm 12\text{ Ma}$ by $^{39}\text{Ar}/^{40}\text{Ar}$ chronology [73], which belong to the putative heavy bombardment period on the lunar surface [74]. The cosmic-ray exposure age of Asuka-881757 implies that this meteorite was exposed in space after launching from the lunar surface for perhaps one million years [75]. According to Ohtani et al. [3], the impact age obtained from $^{39}\text{Ar}/^{40}\text{Ar}$ chronology [73] is thought to represent the time when the shock melt pocket, maskelynite, and the amorphous silica grains containing coesite, stishovite, and quartz were produced. In contrast, the high-pressure silica polymorphs are unlikely to be a product of the impact event when the meteorite was launched from the Moon, based on the space exposure age [75]. This means that the impact event at perhaps one million years ago seems to be energetically lower than that during the putative heavy bombardment period. In addition, their possible formation by impacts to the terrestrial surface can be excluded because of the cutting of a shock vein by a fusion crust (melting textures that formed because of aerodynamic frictional heating during the atmospheric entry). By combining

descriptions of high-pressure silica polymorphs in lunar meteorites with various isotopic ages, we can thus obtain valuable information on the impact processes on the Moon during the putative heavy bombardment period.

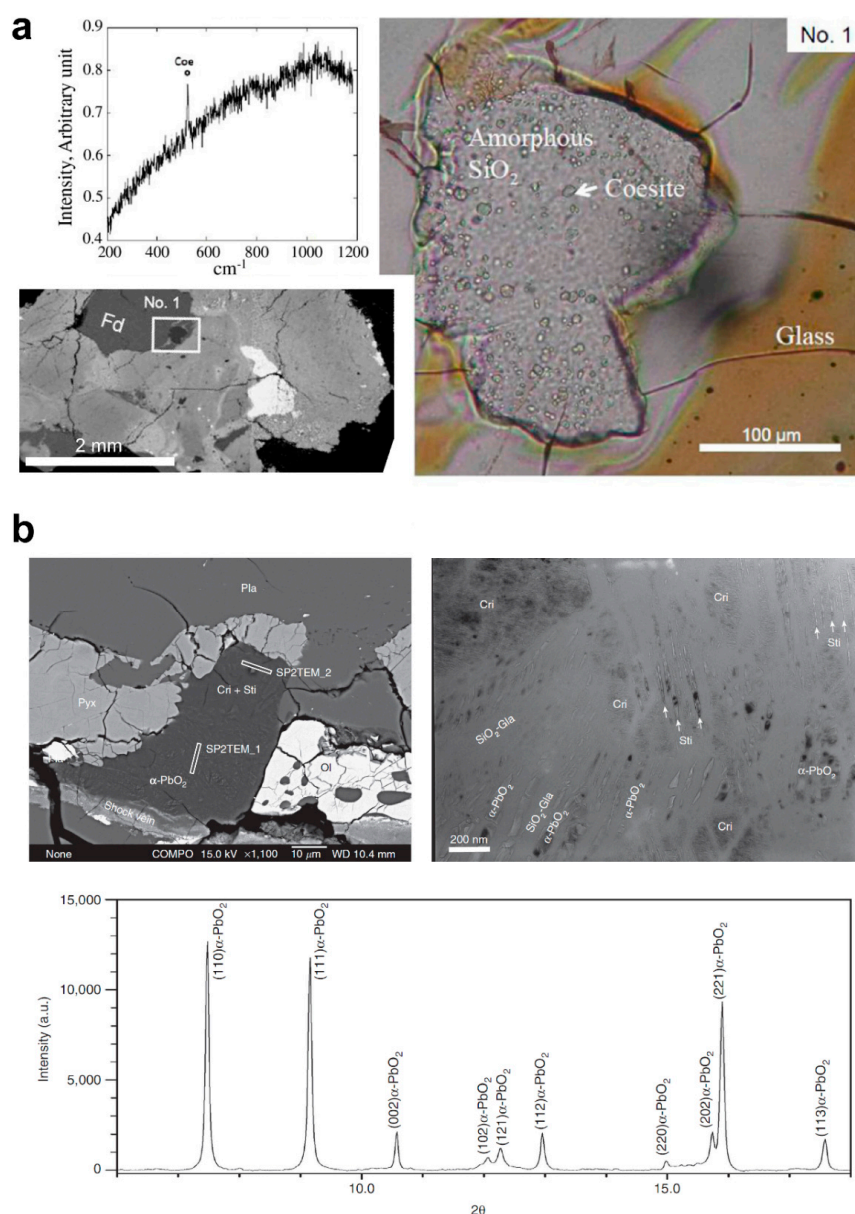


Figure 3. (a) Raman spectrum (left upper), BSE (backscattered electron) image (left bottom), and optical microscopic photograph (right) of silica grain in Asuka-881757. The amorphous silica grain (No. 1) is surrounded by glass with radiating cracks, indicating a volume increase upon pressure release. It contains many coesite (Coe) inclusions that are 1–10 μm in diameter under optical microscopy and is surrounded by feldspar (Fd) in the BSE image. A Raman spectrum of the inclusion shows the typical peak of coesite (521 cm^{-1}) (modified after [3]). (b) BSE image (left upper), transmission electron microscopy (TEM) image, and synchrotron angle dispersive X-ray diffraction (SR-XRD) pattern of the silica grain in NWA 4734. Seifertite ($\alpha\text{-PbO}_2$)-, cristobalite (Cri)-, and stishovite (Sti)-bearing silica grain is enclosed by olivine (Olv), pyroxene (Pyx), and plagioclase (Plg), and lies adjacent to a shock vein in the BSE image. TEM observation reveals that nano-fragments of seifertite, cristobalite, and stishovite exist in the matrix of amorphous silica glass ($\text{SiO}_2\text{-Gla}$). The SR-XRD profile of the silica grain can be indexed into a seifertite structure (modified after [4]).

High-pressure SiO₂ phases that are stable at higher pressures and temperatures than stishovite are called “post-stishovite” (e.g., α -PbO₂-type named seifertite and unnamed baddeleyite-, CaCl₂-, and pyrite-type structures) (Figure 1). The series of post-stishovite phases are considered to be unquenchable when the static pressure releases during experimental decompression, and their existence have been confirmed with XRD analyses [76–78] only during in-situ diamond anvil cell high-pressure and temperature experiments. Until recently, the phase seifertite has been identified in some martian meteorites, as explained in the next chapter. In 2013, Miyahara et al. [4] proved the presence of seifertite in a lunar meteorite, NWA 4734, by field-emission SEM (FE-SEM), SR-XRD, TEM, Raman, and cathodoluminescence (CL) analyses. NWA 4734 is an unbrecciated lunar meteorite with a large amount of highly fractured pyroxene and lath-shaped plagioclase that is partly converted to maskelynite (Figure 3b). Relatively minor silica grains and intersertal silica–feldspar glass, and even smaller amounts of fayalite, ilmenite, baddeleyite, zirconolite, tranquillityite, pyrrhotite, and metal, were also distributed in NWA 4734 (Figure 3b). Shock veins (melting textures due to the impact event) were also seen in NWA 4734, which were either continuous or intersected by other shock veins (Figure 3b). Silica grains (~100 nm in size) were entrained in, close to, or far from the shock veins of NWA 4734. The TEM and SR-XRD analyses of excavated samples from the silica micrograins with a focused ion beam (FIB) system indicated that most of the silica grains in the shock veins were amorphous, but coesite was included in some of them close to the shock vein and occurred as nanometer-sized crystal assemblages (Figure 3b). NWA 4734 also contained tweed-like and lamellae-like textured silica grains, which lay close to and far from the shock veins, respectively. Silica grains with a lamellae-like texture become dominant as the distance from the shock vein increases. The XRD pattern of the tweed-like textured silica grain samples can be indexed to the seifertite structure (Figure 3b). Based on SR-XRD, Raman spectroscopy, and CL measurements, a small amount of stishovite coexists with seifertite. The TEM images and selected area electron diffraction (SAED) patterns of these samples demonstrated that rhomboid or spindle seifertite crystals with dimensions of 50–200 nm by 100–600 nm were surrounded by amorphous silica, and the seifertite crystals appeared to become coarser close to the shock vein. According to the SR-XRD and TEM analyses, the lamellae-like silica textured grains possess twinned α -cristobalite, platelet-shaped stishovite, and seifertite. The stishovite platelets were stacked in the twinned cristobalite under the TEM images. In some cases, amorphous silica was present between the cristobalite and stishovite subgrains.

These results indicate that α -cristobalite, originally crystallized via a rapid cooling process of the lunar magmatism, may have been converted into β -cristobalite by impact events, as indicated by the twinning and the stacking faults. Nucleation took place along the stacking faults under the shock-induced high-pressure and high-temperature conditions, followed by stishovite platelet growth. According to the pressure–temperature phase diagram of SiO₂ [79,80], seifertite is stable at similar pressures, but higher temperatures than stishovite. This is consistent with the conversion of cristobalite into seifertite closer to the shock veins and into stishovite farther away from the shock veins. Moreover, the seifertite in the NWA 4734 crystals became coarser as they were closer to the shock veins. Therefore, seifertite and stishovite may have been formed by the transition from cristobalite during the compression by impact events, where seifertite formed in the hotter regions when compared with stishovite. During decompression, seifertite or other high-pressure silica polymorphs would have been vitrified, resulting in a formation of abundant amorphous silica accompanied with seifertite in NWA 4734. Finally, coesite might have formed in the amorphous silica via rapid-growth processes. Considering the phase diagram [4,80] and impurity contents of aluminum and sodium in the silica grains of NWA 4734, the presence of seifertite would set a constraint for the peak-shock pressure of ~40 GPa or more. An expected temperature of 2573 K or more in the shock veins could also be deduced based on the melting temperature of the KLB-1 peridotite and Allende meteorite, which are chemically similar to NWA 4734. The duration of high-pressure waves required for stishovite formation in NWA 4734 could be estimated by equations related to the grain growth rate and thermal history, which would at least be ~0.1 s. By applying the estimated shock pressure, temperature, and duration to

Rankine-Hugoniot's relation, the impact velocity of the impactor that produced stishovite in NWA 4734 can be obtained [4]. The size of the impactor and the impact crater can be calculated based on Melosh's impact cratering law [81], as discussed in the next section. However, a recent investigation suggested that seifertite metastably appears at a much lower pressure than initially estimated [18].

Seifertite is believed to be unquenchable, that is, it cannot be recovered after an experiment from high-pressure and high-temperature conditions. In addition, this phase is thermodynamically stable at more than ~100 GPa (Figure 1), and heavy impact events that can generate such high pressure conditions are unlikely to occur on the parent bodies of meteorites in the solar system. However, seifertite has been recognized in some lunar and martian shock-metamorphosed meteorites. Recent high-pressure and high-temperature experiments, started from cristobalite with a multi-anvil apparatus and in situ SR-XRD measurements [18], promise new insight into the formation processes of seifertite as a solid-state reaction in meteorites [18]. Kubo et al. [18] revealed the pressure-, temperature-, and time-dependent appearance of seifertite based on the fact that this phase metastably formed during the compression of cristobalite at ~40 GPa and room temperature [80].

According to Kubo et al. [18], cold compressions were first performed for synthetic α -cristobalite and quartz up to ~30 GPa at room temperature, and then heated by ~1450 K with a step of 100 K, where the temperature was kept constant for ~10 to 50 min at each step. During the cold compressions, α -cristobalite was transformed into cristobalite-II and X-I. Subsequent heating experiments caused the transitions of these high-pressure cristobalite phases into metastable seifertite over a wide range of temperatures at pressures greater than ~11 GPa. Finally, a transition of metastable seifertite into the stable stishovite occurred because of further heating. Moreover, this synthetic seifertite could be quenchable down to ambient conditions via the decompression, of which the SR-XRD patterns and lattice parameters corresponded to those reported in meteorites (Table 1). In contrast, quartz was converted into stishovite at approximately 18 GPa and 800 K, and seifertite, did not appear in the high-pressure and high-temperature experiments of quartz up to ~25 GPa and 900 K.

The kinetics of the cristobalite X-I–seifertite and the seifertite–stishovite transitions were analyzed using data obtained from time-resolved SR-XRD measurements. Seifertite formation from cristobalite had very low activation energy (~10 kJ/mol), indicating fast kinetics even at low temperatures, as predicted by [82]. However, the activation energy for the stishovite formation from seifertite was relatively high (~110 kJ/mol). Therefore, seifertite can start to form as a solid-state reaction at rather low temperatures because of its low activation energy. The time–temperature–transformation curves obtained based on these kinetic parameters demonstrated that seifertite formation is time-sensitive, requiring a shock duration time of at least ~0.01 s to even start at a temperature of more than ~2000 K (not completion in the time scale of impact events). In contrast, stishovite formation is temperature-sensitive, requiring temperatures higher than ~1200 to 1500 K to start, and can complete at less than ~2000 K. Considering the solid state-reaction, the existence of seifertite in meteorites constrains the peak pressure of at least ~11 GPa and the duration time of at least ~0.01 s. The impactor size requiring the seifertite formation was inferred to be ~50 to 100 m based on the estimated impact velocities of ~5 to 10 km/s on the Moon [83] and Melosh's impact cratering law [81].

Recent FIB, SR-XRD, and TEM analyses have confirmed the existence of stishovite in Apollo collection sample 15299, returned by the Apollo 15 mission [5]. This is the first report of high-pressure polymorphs from returned lunar samples. Previous reports have indicated that Apollo 15299 is a regolith breccia, and was recovered near the Hadley Valley of the Moon in 1971 (e.g., [84,85]). Apollo 15299 contains relatively low abundances of lithic fragments (mare basalt, gabbro, anorthosite, and pre-existing breccia), mineral fragments (bytownite, clinopyroxene, orthopyroxene, olivine, spinel, and opaques), glass fragments, and glass spheres, with a large portion of glassy matrix. Traces of impact events, such as mafic impact melt breccia and shock veins, were also found in this sample. The mafic melt breccia was composed of fragments of olivine, pyroxene, plagioclase, silica and ilmenite, and glass. Vesicular melt veins of less than 200 μm width crosscut the breccia matrix and mineral fragments. Some silica grains (10–100 μm across) were found in the mafic melt breccia, a part of

which was located in the shock veins. Raman spectroscopy determined that most of the silica grains were quartz, tridymite, or cristobalite based on peak positions in the spectra. One of the silica grains in a shock vein of the breccia matrix consisted of an assemblage of fine quartz and tridymite crystals (~30 µm). Most of the SR-XRD signals of the excavated blocks from this silica grain could be indexed to unit-cell parameters of stishovite and tridymite. A diffraction peak assigned to seifertite appeared in the SR-XRD spectra, although additional peaks would be required to confirm the existence of this phase in the samples. TEM observations indicated that stishovite occurred as needle-like in habit with an ~400 nm grain size, coexisting with poorly crystallized or amorphous silica.

Stishovite, in a shock vein of the breccia matrix, seems to have been transformed from quartz. However, the possibility that the stishovite formed from melt silica cannot be excluded as the needle-shaped habit is considered to be a product because of impact melting [4,86–89]. In any case, the presence of stishovite constrains the shock pressure experienced by Apollo 15299 to be >8 GPa, according to the pressure–temperature phase diagram [90,91] (Figure 1). The relatively high abundance of silica in Apollo 15299 appears to be consistent with KREEP-like basalt or impact melt derived from them. It is possible that Apollo 15299 originated from the Imbrium impact or subsequent local cratering events that occurred in the Procellarum KREEP Terrane (PKT) of the near side of the Moon as the KREEPy rocks were likely concentrated there.

As described above, various types of high-pressure silica polymorphs have been found in lunar meteorites and in the Apollo collection, and appear to be widely distributed in not only the lunar samples, but also materials around the Moon. Therefore, we emphasize that the re-examination of silica in other lunar samples from the viewpoint of a high-pressure phase is important for future micro-mineralogy.

2.3. Alkaline Fluid Activity of the Moon

Aqueous silica polymorphs, originating from fluid activity, are believed to be absent from lunar samples because the Moon is thought to be a water-depleted celestial body [92]. However, various water species (e.g., H₂O ice, OH bound to minerals, and hydrated phases) have been detected at various sites of the lunar surface by recent remote-sensing (e.g., [93,94]). Recent research has discovered the existence of moganite in the lunar meteorite NWA 2727 and indicated the likelihood that this mineral formed as a result of lunar fluid activity [7]. Moganite is a metastable phase of monoclinic SiO₂ in the *I2/a* space group (Table 1). This SiO₂ phase has been synthesized by hydrothermal experiments by high-pressure induced poly-condensation (ca. >100 MPa) and de-hydroxylation of colloidal silicic acid upon changes in pH from 9.5 to 12.0–13.0 at 373–418 K (e.g., [95,96]). On Earth, moganite has been shown to precipitate nano- to micro-crystalline SiO₂ from alkaline fluids only in sedimentary environments that produce high consolidation pressure [97–100]. It readily converts into quartz or dissolves during silica–water interaction at ambient pressure because of its thermochemical instability. Thus, moganite has a limited occurrence in unaltered sedimentary rocks. These findings, reported by previous studies, have become one of the most important pieces of evidence that moganite in NWA 2727 is indigenous to the Moon [7].

NWA 2727 is a gabbroic–basaltic breccia lunar meteorite and is paired with NWA 773, 2977, 3333, 6950, and so on, which together are named the “NWA 773 clan” (e.g., [31,54]). The NWA 773 clan is characterized by KREEP-like compositions with very low Ti, with almost the same crystallization (3.0–3.1 Ga), shock metamorphism ($<2.67 \pm 0.04$ Ga), transition (1–30 Ma), and terrestrial ages (17 ± 1 ka) (e.g., [31,54,101,102]). NWA 2727 consists of an olivine–cumulate (OC) gabbro and pyroxene phyric basalt lithic clasts within a breccia matrix (Figure 4). The OC gabbroic clasts in NWA 2727 contain abundant euhedral olivine and clinopyroxene (0.1–0.5 mm in radius) with minor amounts of anhedral plagioclase [7]. The basaltic clasts are composed of clinopyroxene phenocrysts with a groundmass of clinopyroxene, plagioclase, and small fine-grained silica (10–20 µm in radius). The breccia matrix fills the interstices between these clasts and is composed of numerous fine to coarse grains of the OC gabbro and basalt lithic minerals with small amygdaloidal silica micrograins (Figure 4). Coarse grains

of euhedral silica are also distributed in the felsic lithologies. Continuous shock veins, characterized by impact melt glasses of the constituent minerals with bubbles and flow textures, crosscut both the clasts and the breccia matrix of NWA 2727, indicating their formation after brecciation. Some amygdaloidal silica grains are entrained in the shock veins.

Raman spectroscopy, SR-XRD, and TEM were performed for the silica in the breccia matrix, basaltic clasts, and felsic lithologies (Figure 4) [7]. As a result of these microanalyses, aggregates of moganite, coesite, stishovite, and cristobalite nanoparticles (4.5 nm in average radius) were confirmed in the amygdaloidal silica micrograins of the breccia matrix (Figure 4 and Table 1). In contrast, there was only a quartz phase in the fine-grained silica of the basaltic clasts and only tridymite and cristobalite phases in the euhedral coarse silica grains of the felsic lithologies.

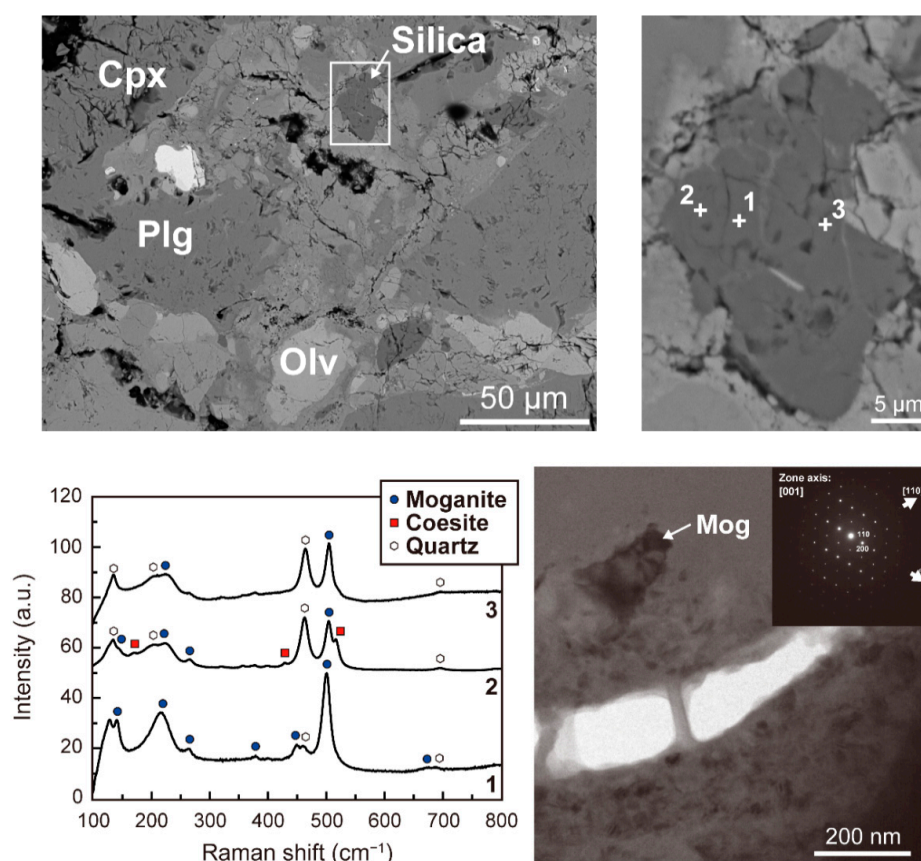


Figure 4. Low-magnification (**left upper**) and high-magnification (**right upper**) BSE images, Raman spectra (**left bottom**), and TEM analytical results of a silica micrograin in NWA 2727. BSE images of NWA 2727 demonstrate that amygdaloidal silica micrograins occur in the breccia matrix of NWA 2727 and coexist with olivine (Olv), clinopyroxene (Cpx), and plagioclase (Plg). Raman signatures of moganite, coesite, and quartz are seen in the silica micrograin. The TEM images and selected area electron diffraction (SAED) patterns of the focused ion beam (FIB)-sliced samples for the silica micrograin indicate the presence of microcrystalline aggregates of moganite nanoparticles with other silica polymorphs (modified after [7]).

Kayama et al. [7] suggested a formation process for lunar moganite based on the comparison of their results with previously reported findings (e.g., [31,54,101,102]). Host rock bodies of the OC gabbroic and basaltic clasts were formed by magmatic processes at the PKT at 2.993 ± 0.032 Ga. Subsequent carbonaceous chondrite collisions occurred there at $<2.67 \pm 0.04$ Ga, resulting in the formation of the breccia bodies on the impact basin. The alkaline water delivered by these collisions is highly likely to have been captured inside the breccia bodies via consolidation. On the sunlit

surface (363–399 K), moganite could have formed via precipitation from the captured alkaline water in the breccia matrix. Simultaneously, the captured water was cold-trapped as H₂O ice in the subsurface of the brecciated bodies. The NWA 773 clan was launched from the surface of the brecciated bodies by the most recent impact event at 8–22 GPa and >673 K. These shock conditions could be constrained by the coexistence of moganite with coesite, stishovite, and cristobalite in the amygdaloidal silica micrograins of the breccia matrix in NWA 2727, according to the SiO₂ phase diagram (Figure 1). This impact event was possibly generated at ca. 1–30 Ma. Finally, the NWA 773 clan may have fallen to Earth at a terrestrial age of 17 ± 1 ka. Such H₂O ice cold-trapped in the subsurface is expected to still remain today as it can theoretically survive over billions of years [103]. Assuming the moganite precipitation model, an amount of at least 0.6 wt % of H₂O ice in the subsurface was calculated [7]. This value is in excellent agreement with concentrations of H₂O ice on the surface of the lunar poles estimated from spacecraft observations (e.g., [94,104]). Therefore, the subsurface H₂O ice is one of the most abundant water resources for future lunar explorations.

As introduced here, moganite has been overlooked for many years, but it is an important silica polymorph in extraterrestrial materials that can be used as a marker for the existence of H₂O ice in the Moon's subsurface. Further discoveries of such aqueous silica polymorphs, including moganite from other lunar samples and/or future sample return programs, might provide new insight into water on the Moon.

3. Mars

3.1. Martian Igneous Process

Martian meteorites are launched from Mars as a result of heavy impact and the ejected fragments are attracted toward Earth. In this decade, the number of martian meteorites has drastically increased because of collecting programs in hot desert areas, currently reaching over 200 meteorites [105]. Martian meteorites have mostly formed via igneous processes and can be classified into five groups: shergottite, nakhlite, chassignite, orthopyroxenite, and basaltic breccia. Their igneous ages vary from the 4.5 Ga of Allan Hills (ALH) 84001 to as young as 180 Ma shergottite. Therefore, they reveal the environmental history of Mars across various periods of time (e.g., [106,107]). Martian meteorites have experienced heavy impact events at least in the moment of ejection from Mars, as indicated by the transformation of plagioclase into maskelynite [108]. Igneous or secondary silica has been reported in most types of martian meteorites.

Only one meteorite has been classified as orthopyroxenite, Allan Hills (ALH) 84001. This martian meteorite (1931 g), found in Antarctica in 1984, has quite an old radiogenic age of 4.5–4.0 Ga and a cosmic ray exposure age of 15 Ma [106]. The silica in this meteorite is associated with various occurrences; igneous silica has been reported as the intergrowth with plagioclase, which has currently transformed into maskelynite by shock metamorphism [109]. This meteorite is unique because of the existence of carbonates, which are often mixed with silica. The amount of carbonates in the meteorite is estimated to be around 0.46% to 1.0% of the rock [110–112]. Silica glasses are thought to be contemporaneously formed with carbonates (Figure 5a) [109,113–120]. Furthermore, silica occurs as patchy or vein-like structures in the fractures of pyroxene grains [121–123]. Silica phases in the meteorite have been identified by mineralogical investigations. Cooney et al. [124] analyzed these silica grains using Raman spectroscopy, which showed a broad feature with a weak sharp peak at 462 cm⁻¹, probably less than 5% of quartz, and the peak at 400 cm⁻¹ may come from trace amounts of tridymite. Formational and alteration processes are still under discussion. The existence of feldspathic and silica glasses constrains the relative timing of impact events and carbonate deposition in the meteorite [119]. Melwani Daswani et al. [120] computed their results using a one-dimensional transport thermochemical model and suggested that the alteration process produced carbonate assemblages, including amorphous silica. Therefore, silica materials in ALH84001 were formed in association with aqueous alteration and impact events.

Nakhlites are mostly composed of clinopyroxene formed at 1.3 Ga. Currently, 19 meteorites have been classified into this group. Some nakhlites that have experienced aqueous alteration contain carbonate veins and altered minerals such as iddingsite (e.g., [6,125]). Silica in Nakhla meteorites (Nakhlite) is also considered to be an alteration product [6]. Imae et al. [126] identified silica grains such as tridymite in Yamato 000593 using a Gandolfi camera, but did not discuss their origin. A representative report of hydrothermally precipitated silica was later introduced.

Shergottites are the largest group of martian meteorites. This group is sub-classified into three types: basaltic, olivinephyric, and lherzolitic, and can be further subdivided into three types by incompatible element features (enriched, depleted, and intermediate). These features indicate a wide variation in igneous process [106,127]. Furthermore, shergottites have a wide range of crystallization age of about 500–200 Ma [106] and consist of the constituent minerals of pyroxene, olivine, and plagioclase that were transformed into maskelynite by the impact event (igneous plagioclase with minor amorphization has been reported from two shergottites; [128]). Fine-grained silica, including silica glass, is part of the mesostasis of shergottites [129–137]. NWA 5298 shows relatively large grains of silica polymorphs up to 0.4 mm in size [138,139]. A shergottite named Los Angeles has large grains (up to 1 mm in size) of silica [140,141]. In Los Angeles, silica is an intergrowth with anorthoclase in late stage residual melts and transformed by secondary impact events (Figure 5b). Almost all identified silica consists of high-pressure polymorphs formed by shock metamorphism together with pre-existing low-pressure silica polymorphs [25,26,71,142,143], described in later section). Quartz and tridymite have been identified in Dhofar 378 using Raman spectroscopy [144]. Coesite has also been reported from NWA 8675 [145]. Late stage products of fayalite, hedenbergite, and pyroxferroite are present in the evolved shergottites of Zagami [146,147], Los Angeles [140,148–150], QUE 94201 [151], Ksar Ghilane 002 [152,153], NWA 2800 [154], and NWA 7320 [155]. Pyroxferroite is a metastable phase [156] that occurs marginally on pyroxene grains or in the mesostasis, and is currently symplectite (pyroxene–fayalite–silica) that might have been formed by a later thermal event. The formation event is still under debate, but was probably not affected by shock metamorphism [151].

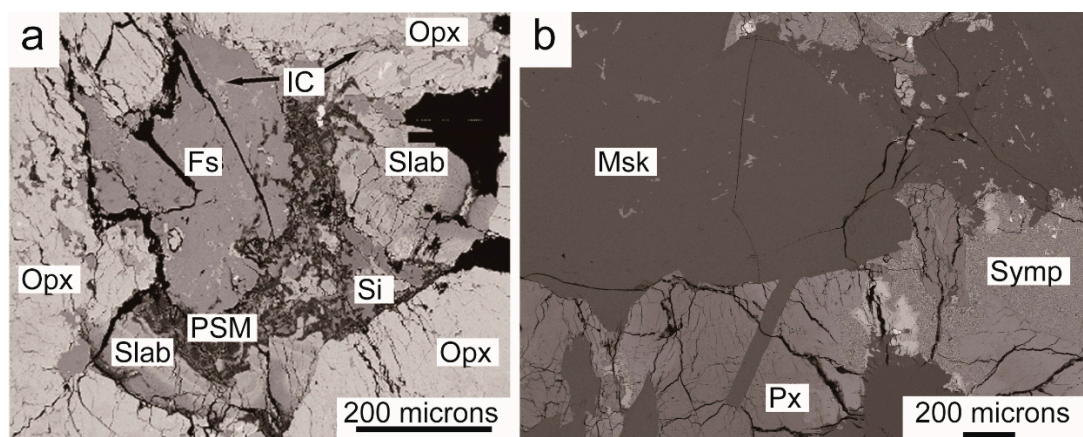


Figure 5. Occurrence of silica in martian meteorites. (a) Silica in association with carbonate materials in ALH84001 (image from [117]). (b) Pyroxferroite break down products (pyroxene–olivine–SiO₂) in the Los Angeles shergottite. Slab: Slab carbonates, Opx: Orthopyroxene, Fs: Feldspathic glass, IC: Interstitial carbonate, PSM: Post slab magnesite, Si: Silica glass, Msk: Maskelynite, Px: Pyroxene, Symp: Symplectite.

Only three meteorites (Chassigny, NWA 2737, and NWA 8695) have been classified in the Chassignite group. The dominant mineral in this group of meteorites is mostly olivine, with ~5% of pyroxene. Recently, new types of rocks (basaltic breccia and martian regolith) from Mars

have been added to the martian meteorite collections [157,158]. These are known as “black beauty” and are 10 times richer in water, whereas silica has not been identified from these two types of martian meteorites.

Martian meteorites have been launched from several places on Mars according to the formation and ejection ages [106]. However, recent martian explorations have not found similar materials on Mars, indicating that martian meteorites are not representative of martian surface materials. Silica was observed by the martian exploration rovers Spirit and Opportunity and the Mars Science Laboratory’s Curiosity. Spirit identified opaline silica deposit in the Gusev crater [8], which seems to form similar deposits as terrestrial silica, for example, at hot springs in Chile [159]. Curiosity found ~14 wt % of tridymite, ~2 wt % cristobalite, and silica-rich amorphous (opal-A and opal-CT) in the drill sample of the sedimentary rocks in the Gale crater according to an X-ray diffraction instrument [160].

Silica in martian materials formed via igneous processes, shock metamorphism, and hydrothermal alteration. Martian meteorites have been overprinted by shock metamorphism, at least during ejection from Mars. However, most of the silica has not been directly identified by mineralogical analysis, especially from the viewpoint of micro-mineralogy. Remote-sensing data show aqueous activity on Mars, as well as martian meteorites, thus, silica in martian meteorites is important for solving questions about past and present hydrous activity on Mars, as discussed later.

3.2. Shock Metamorphism on Mars

Shergotty, which fell in 1865 near Shergahti in Bihar State, India, is texturally and mineralogically similar to terrestrial diabases, and a martian meteorite family petrologically similar to it is called “shergottite” (e.g., Shergotty, Tissint, Zagami, NWA 480, 856, 1068, 2975, 4468, and SaU 005). Almost all shergottites record a trace of heavy impact events (maskelynite and melting textures) on Mars. Shergotty is mainly composed of prism-shaped pyroxene up to 1 cm size and lath-like and interstitial maskelynite. It also contains minor minerals of fayalite, Ti-magnetite, and large silica grains (>150 nm), most of which are wedge shaped [19]. The silica grains are either enclosed in clinopyroxene or exist among clinopyroxene, mesostasis, and maskelynite [26]. Many of the silica grains are surrounded by radiating cracks that were caused by a rapid increase of the volume with decompression. TEM observations and SAED analysis confirmed, for the first time, the existence of post-stishovite SiO₂ with an α -PbO₂ structure in the martian meteorite Shergotty [19]. Ten years later, this high-pressure SiO₂ phase has been named “seifertite”, based on more accurate data [25].

In general, martian meteorites have been subject to higher shock pressure during impact events on the parent body when compared with other meteorites such as lunar meteorites and carbonaceous chondrites (e.g., [1,2,17,21]). Therefore, various types of high-pressure minerals, which have already been named, have been reported in martian meteorites (e.g., ringwoodite, akimotoite, and majorite), and new high-pressure minerals have been found in them (e.g., tissintite, liebermannite, and zagamiite) [17,161]. In the case of silica, Sharp et al. [19] and El Goresy et al. [25,26] reported the first discoveries of an α -PbO₂-type (named seifertite) and a baddeleyite-type (unnamed) high-pressure SiO₂ phase from martian meteorites.

Sharp et al. [19] investigated the morphology, crystallinity, and structure of the silica grains in Shergotty by using FE-SEM and TEM. Lamellae textures of the silica grains were observed using FE-SEM. The three zone-axes SAED patterns of crystalline domains in the silica grains were inconsistent with known SiO₂ polymorphs, including post-stishovite, at the time. Following this initial characterization of seifertite in Shergottite, El Goresy et al. [25] acquired SAED and XRD diffraction data of the silica grains in Shergotty that could be interpreted in terms of α -PbO₂-type structure (Table 1), and they named it “seifertite”. The large seifertite-bearing silica grains have a typical pre-shock morphology and habit of tridymite or cristobalite, one of them seemed to be igneous SiO₂ phase in Shergotty before shock metamorphism [19,25]. Considering the kinetic data reported in [18], it is reasonable to suppose that cristobalite was a preexisting mineral before the impact, because it transforms into seifertite at relatively low pressures. Mineralogical and petrological descriptions of

seifertite in Shergotty have also been reported in [132], where shock pressure and temperature were estimated based on mineral paragenesis of various high-pressure minerals including silica.

Post-stishovite with a baddeleyite-type structure has also been discovered from the silica grains in Shergotty [26]. Previous crystallographic experimental investigations indicated that α -PbO₂-like silica (space group *Pbcn* or *Pnc2*) is stable above 70 GPa and theoretically above 85 GPa, and is related to the baddeleyite-type SiO₂ structure by its seven-coordination of oxygen (e.g., [26,80,162]). Most silica in Shergotty occurs as wedge-shaped coarse crystals (150 to 900 μ m), and are surrounded by pervasive radiating cracks [26]. BSE images of every silica grain obtained by FE-SEM showed mosaics of domains (10 to 60 μ m) with orthogonal sets of lamellae.

XRD analysis of the silica grains showed characteristic signals of both a broad halo and reflections. The broad halo belonged to amorphous silica. Some of the XRD reflections were consistent with a stishovite structure. However, most of the XRD reflections were unsuitable for any known silica polymorphs, and could be indexed to a monoclinic unit cell with a cell parameter that has not been recognized in natural silica polymorphs [26]. This monoclinic phase had a calculated density higher than stishovite, that is, post-stishovite produced by impact events on Mars. The calculated intensities of the reflections for baddeleyite-structured SiO₂ were similar to the observed monoclinic phase (Table 1). The TEM observations revealed that the silica grains had intergrowths of crystalline and amorphous lamellae. The SAED patterns of the crystalline lamellae corresponded to a mixture of stishovite and cristobalite structures. However, baddeleyite-type SiO₂ was not seen in the SAED patterns of the silica grains, although it was identified in the XRD analysis. This may be caused by the high instability of baddeleyite-type SiO₂ during sample preparation for TEM. Moreover, this baddeleyite-type SiO₂ appeared to be metastable and readily changed to a more stable, low-pressure phase because of its sensitivity to X-ray and electron irradiation. Although uncertainties remain regarding the formation process of baddeleyite-type SiO₂ instead of the expected α -PbO₂-type phase (e.g., [76,163,164]), El Goresy et al. [26] speculated that small amounts of impurities (such as Na₂O and Al₂O₃) and heterogeneous stress distribution during compression could be factors preserving the baddeleyite-type SiO₂ phase from destruction. However, this baddeleyite-type SiO₂ has yet to be accepted as a new mineral as it has not been well-characterized, and for this reason it has not been given a name. Thus, further crystallographic research on this silica phase in martian meteorites is timely. Shock melt pockets in Shergotty and other martian meteorites also possess intergrowths of stishovite with a (Na,Ca)-hexaluminosilicate mineral (hexagonal barium ferrite-type) [(Ca_xNa_{1-x})Al_{3+x}Si_{3-x}O₁₁], as described at the end of this chapter.

In martian meteorites, other high-pressure silica phases have also been reported. Stishovite was discovered in Zagami using TEM analysis [86–88]. Zagami (fell in 1962 in Nigeria) is a basaltic shergottite and is composed of several different lithologies. The basaltic lithology (called fine-grained lithology) is petrologically similar to Shergotty, and is characterized by a foliation of pyroxene and maskelynite that is crosscut by shock veins.

Langenhorst and Poirier [86,87] examined mineral assemblages in shock veins of the basaltic lithology of Zagami. TEM observation of the wider shock veins with a thickness of 100 μ m indicated a tiny mineral phase embedded in a glassy matrix [86]. One of the mineral phases was needle-shaped silica. SAED patterns and TEM images consistently established this phase to be stishovite. Stishovite (10 to 100 nm in size) mostly occurred as isolated crystallites in the glassy matrix. Some stishovite coexisted with the hollandite-type KAlSi₃O₈ (liebermannite) as rounded polycrystalline aggregates. This assemblage is considered to have been crystallized from a melt at a high shock pressure. Amorphous grains of silicate perovskite were surrounded by stishovite and wüstite. On the basis of mineralogical description and thermodynamic calculation of the shock vein, most of the mineral phases, including silicate perovskite, directly crystallized from shock-induced melt at high pressures and very high temperatures, and then the silicate perovskite became amorphous during the decompression. Finally, silicate perovskite changed into the lower pressure assemblage of stishovite and wüstite because of solid-state diffusion at its grain boundaries. Additionally, CAS-phases

intergrown with stishovite have been observed in the shock melt pockets of Zagami [88]. This CAS phase is now referred to as zagamiite (IMA No. 2015-022a, as described by [165]).

Tissint is a unique martian meteorite, because its fall was witnessed by many people (2011 in Morocco), so the rock is thus unweathered. Tissint is a heavily shocked olivine–phyric shergottite composed of subhedral to euhedral olivine (up to 2 mm in size) in a groundmass of smaller olivine, pyroxene, maskelynite, and minor minerals (Ti–chromite to ulvöspinel, ilmenite, merrillite). Shock melt pockets and shock veins contained various high-pressure minerals, for example, ringwoodite, tissintite, and stishovite [166,167].

Raman spectroscopy and SEM imaging suggested the existence of stishovite associated with olivine inside shock melt pockets [166]. However, EMPA analysis could not be performed for stishovite as the grains were too small (1 to 2 μm microcrystalline of stishovite + olivine). According to Walton et al. [167], within a shock vein of 120 μm in thickness, sparse anhedral crystals of clinopyroxene and ringwoodite and tiny needles of stishovite were embedded in a predominantly amorphous matrix and represented a metastable assemblage (stishovite + clinopyroxene + glass in shock veins) crystallized via rapid quenching during decompression.

In other martian meteorites, stishovite, seifertite, and HP silica glass have been observed using various microanalyses. Stishovite was first reported in Los Angeles by Walton and Spray [168] as small (10 to 20 μm size), needle-shape crystals that were quench-crystallized in shock melt pockets. Beck et al. [88] reported that a new mineral of the (Na,Ca)–hexaluminosilicate phase (hexagonal barium ferrite-type) $[(\text{Ca}_x\text{Na}_{1-x})\text{Al}_{3+x}\text{Si}_{3-x}\text{O}_{11}]$, referred to as the CAS-phase, was intimately intergrown with stishovite in the shock melt pockets of NWA 480, 856, 1068, and Sayh Al Uhaymir 005, similar to the cases of Shergotty and Zagami. Chennaoui Aoudjehane et al. [141] studied silica in shergottites NWA 480, NWA 856, Zagami, Shergotty, and Los Angeles using SEM and CL, and confirmed stishovite in all meteorites, with the exception of Los Angeles. According to the phase diagram of a basaltic composition at high pressures and temperatures, stishovite and CAS-phase appear as liquidus phases in the shock-induced melt. El Goresy et al. [143] found oblong polycrystalline stishovite with an orthogonal intergrowth of presumable post-stishovite (either residual seifertite, or monoclinic ZrO_2 -type silica polymorph) inverted from stishovite in NWA 480. In the shock vein of NWA 856, they also encountered a coarse silica grain with a faulted orthogonal pattern of seifertite. He et al. [169] described irregularly shaped silica grains between plagioclase, clinopyroxene, and Fe–Ti oxides in NWA 2975, which according to Raman spectroscopy, were stishovite. Furthermore, such lamellae-textured intergrowths were present in silica grains that might be a mixture of seifertite and HP silica glass, based on the SEM observations. In addition to these investigations, Boonsue and Spray [170] reported stishovite in NWA 4468. As introduced in this section, high-pressure silica polymorphs are a valuable recorder of impact events on Mars. A mineral assemblage of high-pressure minerals, including silica, gives us hints to constrain the shock pressure and temperature of those impact events, and in deducing the impactor and crater sizes based on these factors. This information hints at the birthplace of each martian meteorite.

3.3. Acid Fluid Activity of Mars

Minerals precipitated from Mars's liquid water have been reported in some martian meteorites, and provide valuable information on the martian hydrosphere, including its temperature, elemental composition, pH, Eh (i.e., redox potential), and longevity (e.g., [6,171–175]). Recently, Lee et al. [6] confirmed the existence of opal-A nanoparticles in the martian meteorite, Nakhla. The fall of the Nakhla meteorites in Egypt in 1911 were recorded, and some of the fragments were collected by a researcher. Nakhla is pristine and free from terrestrial contamination because of its rapid recovery, therefore, alteration products described from Nakhla can be inferred to be martian in origin. Nakhla is a cumulate clinopyroxenite with small amounts of olivine, intercumulate mesostasis, and minor iddingsite (1 wt %), and is similar to other martian meteorites called nakhlites. A series of cumulate clinopyroxenitic martian meteorites is referred to as “nakhlite” (e.g., NWA 998, MIL 03346,

and Yamato 000593), and most of them consist of clinopyroxene, olivine, and water-based minerals such as iddingsite. In Nakhla, this alteration product from olivine was a result of water–mineral interactions and is a mixture of hydrous Fe–Mg silicate (phyllosilicate), carbonate, sulfate, and halide. This alteration product seems to be indigenous to Mars, rather than terrestrial weathering as it is crosscut by the fusion crust and its radiometric formation age is 633 ± 23 Ma. Recent TEM analyses of the iddingsite from Nakhla have proven the presence of opal-A (~12 nm in diameter) in the Fe–Mg silicate, which is thought to have been formed by martian fluid activity.

Scanning TEM (STEM)-high angle annular dark-field (HAADF) imaging showed that the Fe–Mg silicate is comprised of closely packed particles that are circular to oval in shape. The cores ranged in diameter from 5 nm to 29 nm. As a result of STEM-electron energy loss spectroscopy (EELS) and energy dispersive X-ray (EDX) measurements, one of the largest cores corresponded to pure silica nanoparticles (Figure 6). Orange-colored discontinuous iddingsite veins were readily observed in a thin section of Nakhla using a plane polarized transmitted optical microscope, and were distributed within all olivine grains (300 to 1000 μm in size) of Nakhla [6]. Most of them were located—with a few ten micrometers in length and 1.9 to 7.0 μm —along the olivine–augite grain boundaries, and rarely within augite, and Fe–Mg silicate, siderite, and ferric (oxy)hydroxide were included in the iddingsite veins (Figure 6). The SAED patterns of the silica nanoparticles showed a broad diffuse ring assigned to amorphous SiO_2 (Figure 6). According to previous studies that assumed a 10 wt % of bulk water of Fe–Mg silicate of nakhlite [172,176–180], these silica nanoparticles were most probably opal-A (amorphous $\text{SiO}_2 \cdot n\text{H}_2\text{O}$) [6]. Narrow rings in the SAED pattern were consistent with two-line ferrihydrite ($\text{Fe}_{8.2}\text{O}_{8.5}(\text{OH})_{7.4} + 3\text{H}_2\text{O}$), suggesting its coexistence with opal-A nanoparticles. In fact, the TEM observation revealed that each opal-A nanoparticle was enclosed within a ferrihydrite shell (Figure 6).

According to these micro-mineralogical descriptions [6], olivine changed into iddingsite in the host rocks of Nakhla during discrete events with the variation of pH, Eh, and the chemical composition of solutions, rather than from a single evolving fluid. During the discrete fluid activities, Fe–Mg silicate formed first, then siderite grew by replacement, and finally, ferric (oxy)hydroxide was produced by the oxidation of the carbonate; preexisting olivine, a precursor of Fe–Mg silicate, was dissolved during initial the water–mineral interaction, and simultaneously, opal-A was precipitated in the host rock of Nakhla, in agreement with the previous report [181]. The initial acidic ($\text{pH} \leq 4$) and oxidizing fluid activities were considered to have occurred according to the previous chemical analyses of the Fe–Mg silicate and spacecraft observations (e.g., [8,175,182]). The fluids dissolved olivine and precipitated opal-A and ferrihydrite. The secondary fluid solutions had a high pH and low Eh, and introduced siderite into the iddingsite veins of Nakhla, which were formed by the replacement of olivine and the opal-A plus ferrihydrite. Findings of opal-A coexisting with ferrihydrite in the Nakhla iddingsite are in good agreement with the result obtained from theoretical [183] and laboratory experiments of silica under martian conditions [184,185]. The final fluid activity recorded by the iddingsite veins was the partial oxidation of siderite to a ferric (oxy)hydroxide, which probably took place on Mars.

Furthermore, spectroscopic spacecraft observations of the martian surface by orbiters and landers have also discovered extensive deposits of hydrous and amorphous opaline silica on the surface of Mars (e.g., [186–188]). Although opal-A has been recognized in only one of the nakhlite samples, amorphous and hydrous silica such as opal-A may be widespread on Mars. Therefore, Lee et al. [6] interpreted that Amazonian clinopyroxenite lava flow/sill seemed to be the martian host of opaline silica, and Syrtis Major (hosts a volcanic hydrothermal deposit of silica) was proposed as a source of the nakhlites [189]. As shown here and above, aqueous silica polymorphs in extraterrestrial materials, such as opal-A in the martian meteorite Nakhla and moganite in the lunar meteorite NWA 2727, are indicative of fluid activities on the parent bodies.

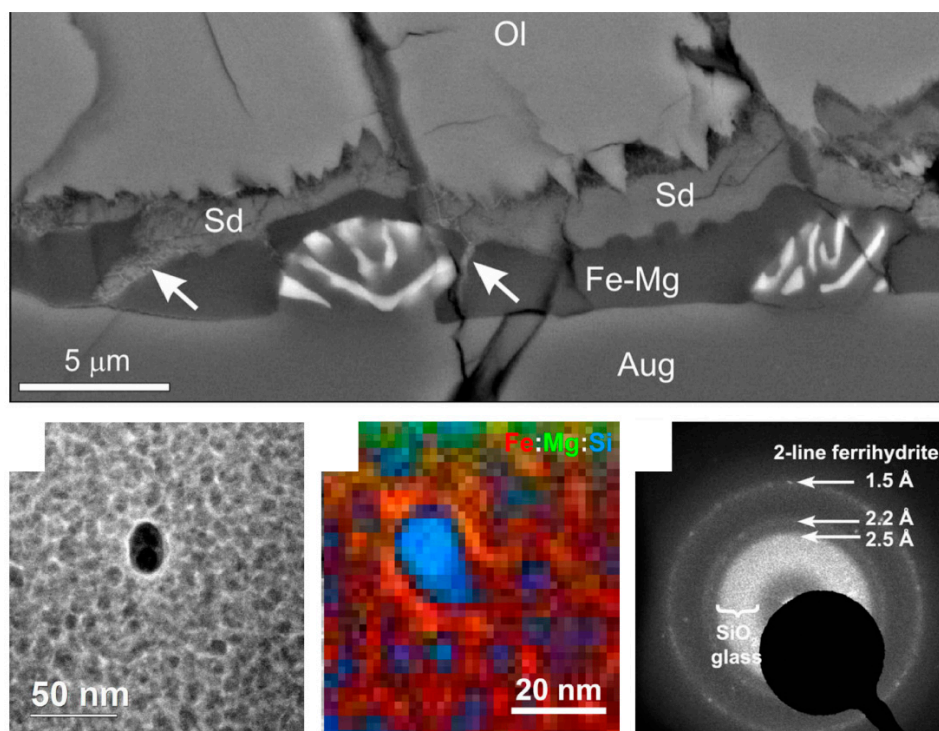


Figure 6. BSE images of iddingsite veins within grains of olivine (Ol) (top); the high angle annular dark-field (HAADF) scanning TEM (STEM) image of nanoparticles in the Fe–Mg silicate (left bottom); false-color elemental map of Fe, Mg, and Si (middle bottom) obtained from the EELS spectrum imaging of the nanoparticles; and the SAED pattern from a group of nanoparticles (right bottom). The BSE image demonstrated that the iddingsite veins contained Fe–Mg silicate (Fe–Mg) and siderite (Sd), and lay at the interface between olivine and augite (Aug). The HAADF STEM observation of the Fe–Mg silicate revealed a large amount of nanoparticles. Pure silica nanoparticles (aqueous blue) were found in the Fe–Mg silicate, using the false-color silicate elemental map, and may be opal-A enclosed within ferrihydrite, based on the results of the SAED analysis (modified after [6]).

4. Conclusions

The micro-mineralogy of silica in lunar and martian materials provides new insight into geological events in the host celestial bodies. Of course, to achieve this purpose, it is essential to clarify the mineralogical properties of micro- to nanometer-sized silica crystals using Raman microscopy, SR-XRD, TEM, and EBSD. However, some works on extraterrestrial materials, including lunar and martian materials, have only reported silica based on conventional observations, and did not determine the type of silica polymorphs, especially for the fine silica grains, by using advanced microanalyses. Here, we introduced representative and important micro-mineralogical studies of silica polymorphs that were formed by igneous, shock metamorphic, and fluid processes on the Moon and Mars. Furthermore, we reviewed the details from the viewpoints of the discovery from lunar and martian materials, the formation processes, the implications for planetary science, and future prospects in the field of micro-mineralogy in each section:

(1) Lunar igneous process

Igneous silica polymorphs are known as cristobalite, tridymite, and quartz. On the basis of micro-mineralogical investigations of the Apollo collections and lunar meteorites, silica is one of the major minerals in late-stage products such as granitic rocks. A combination of micro-mineralogical and remote-sensing data can provide hints to determine the candidates of silicic volcanism that formed on the lunar surface.

(2) Shock metamorphism on the Moon

Recently, high-pressure silica polymorphs such as coesite, stishovite, and seifertite have been discovered from a part of lunar meteorites and an Apollo collection, although they were previously believed to be absent from the lunar materials because of their elimination from impact-induced volatilization and the difficulty in finding fine-grained high-pressure silica using conventional methods. Of course, various types of high-pressure silica polymorphs are likely to be included in other parts of lunar meteorites and in the Apollo and Luna collections, therefore, further findings of high-pressure silica polymorphs in future micro-mineralogical studies are important for understanding impact events on the Moon.

(3) Alkali fluid activity of the Moon

Aqueous silica polymorphs, formed by fluid activity, were believed to be absent from lunar samples. However, a recent study reported the presence of moganite in the lunar meteorite of NWA 2727 and demonstrated the likelihood that this silica was precipitated from lunar fluid activity. An amount of at least 0.6 wt % of H₂O liquid is theoretically necessary for moganite precipitation and would accumulate as ice in the subsurface. Therefore, the subsurface H₂O ice is one of the most abundant water resources for future lunar explorations.

(4) Martian igneous process

Most and various types of martian meteorites contain silica polymorphs, however, micro-mineralogical investigation in this area seems to be limited. Therefore, types of some martian silica have yet to be identified. More detailed works on the micro-mineralogy of silica could assist in answering questions regarding igneous processes on Mars.

(5) Shock metamorphism on Mars

Martian meteorites are known to have been affected by heavy impact events. For this reason, various types of high-pressure minerals, including silica, have been discovered from them for the first time, and one of the high-pressure silica phases has been named seifertite. A possible baddeleyite-type high-pressure SiO₂ phase has also been reported in a martian meteorite. The presence of high-pressure silica polymorphs sets a constraint for peak-shock pressure and shock duration time on the celestial bodies, and provides us with clues to deduce the impactor and crater sizes, and the birthplace of each martian meteorite, as well as the lunar meteorites.

(6) Acid fluid activity of Mars

The existence of opal-A nanoparticles, precipitated from Mars's liquid water, has been confirmed in the martian meteorite, Nakhla. This finding provides valuable information on the martian hydrosphere. Moreover, spacecraft observations have also discovered extensive deposits of hydrous and amorphous opaline silica on the surface of Mars. Aqueous silica polymorphs in extraterrestrial materials such as opal-A in Nakhla and moganite in NWA 2727 are indicative of fluid activities on the parent bodies.

In the near future, the micro-mineralogy of igneous silica in lunar and martian materials (that have yet to be fully studied) will definitely give us new insight into the thermal histories of the Moon and Mars. Furthermore, new silica polymorphs (e.g., CaCl₂- and pyrite-type) and the unnamed baddeleyite-type will likely be discovered from lunar and martian materials that have experienced heavy impact events. Additionally, the martian aqueous silica polymorphs (e.g., moganite, opal-A, and maybe opal-CT) will make the fluid activities of the Moon and Mars clear. Other lunar and martian meteorites, the Apollo and Luna collections, and other types of meteorites such as eucrite and carbonaceous/ordinary chondrites should be investigated using advanced microanalysis for the micro-mineralogy of silica.

Author Contributions: M.K. outlined and designed this article, and also wrote the paper relevant to shock metamorphic and fluid activity martian igneous silica, respectively. All authors participated in discussing the manuscript and checking all content.

Funding: This work was partly supported by the Astrobiology Center of National Institutes of Natural Sciences (NINS) (Grant Number AB291023) and Kurita Water and Environment Foundation (Grant Number 17D006) to T.N.

Acknowledgments: We would like to thank Jens Götze (TU Bergakademie Freiberg, Institute of Mineralogy,) for inviting Masahiro Kayama to submit to the Special Issue “Mineralogy of Quartz and Silica Minerals” of “Minerals”. We are deeply indebted to Loker He (Assistant Editor, Minerals) for coordinating our paper. This work was partly supported by the Astrobiology Center of National Institutes of Natural Sciences (NINS) (Grant Number AB291023) and Kurita Water and Environment Foundation (Grant Number 17D006) to T.N.

Conflicts of Interest: The authors declare no conflict of interest.

References

1. Papike, J.J. Comparative planetary mineralogy: Chemistry of melt-derived pyroxene, feldspar, and olivine. In *Planetary Materials; Reviews in Mineralogy & Geochemistry*; Papike, J.J., Ed.; Mineralogical Society of America: Chantilly, VA, USA, 1998; pp. 7-1–7-11.
2. Lucey, P.; Korotev, R.L.; Gillis, J.J.; Taylor, L.A.; Lawrence, D.; Campbell, B.A.; Elphic, R.; Feldman, B.; Hood, L.L.; Hunten, D.; et al. Understanding the lunar surface and space-moon interactions. In *New Views of the Moon, Reviews in Mineralogy & Geochemistry*; Jolliff, B.L., Wieczorek, M.A., Shearer, C.K., Neal, C.R., Eds.; Mineralogical Society of America: Chantilly, VA, USA, 2006; pp. 83–220.
3. Ohtani, E.; Ozawa, S.; Miyahara, M.; Ito, Y.; Mikouchi, T.; Kimura, M.; Arai, T.; Sato, K.; Hiraga, K. Coesite and stishovite in a shocked lunar meteorite, Asuka-881757, and impact events in lunar surface. *Proc. Natl. Acad. Sci. USA* **2011**, *108*, 463–466. [[CrossRef](#)] [[PubMed](#)]
4. Miyahara, M.; Kaneko, S.; Ohtani, E.; Sakai, T.; Nagase, T.; Kayama, M.; Nishido, H.; Hirao, N. Discovery of seifertite in a shocked lunar meteorite. *Nat. Commun.* **2013**, *4*, 1737. [[CrossRef](#)] [[PubMed](#)]
5. Kaneko, S.; Miyahara, M.; Ohtani, E.; Arai, T.; Hirao, N.; Sato, K. Discovery of stishovite in Apollo 15299 sample. *Am. Mineral.* **2015**, *100*, 1308–1311. [[CrossRef](#)]
6. Lee, M.R.; MacLaren, I.; Andersson, S.M.L.; Kovács, A.; Tomkinson, T.; Mark, D.F.; Smith, C.L. Opal-A in the Nakhla meteorite: A tracer of ephemeral liquid water in the Amazonian crust of Mars. *Meteorit. Planet. Sci.* **2015**, *50*, 1362–1377. [[CrossRef](#)]
7. Kayama, M.; Tomioka, N.; Ohtani, E.; Seto, Y.; Nagaoka, H.; Götze, J.; Miyake, A.; Ozawa, S.; Sekine, T.; Miyahara, M.; et al. Discovery of moganite in a lunar meteorite as a trace of H₂O ice in the Moon’s regolith. *Sci. Adv.* **2018**, *4*, eaar4378. [[CrossRef](#)] [[PubMed](#)]
8. Squyres, S.W.; Arvidson, R.E.; Ruff, S.; Gellert, R.; Morris, R.V.; Ming, D.W.; Crumpler, L.; Farmer, J.D.; Des Marais, D.J.; Yen, A.; et al. Detection of silica-rich deposits on Mars. *Science* **2008**, *320*, 1063–1067. [[CrossRef](#)] [[PubMed](#)]
9. Hsu, H.-W.; Postberg, F.; Sekine, Y.; Shibuya, T.; Kempf, S.; Horányi, M.; Juhász, A.; Altobelli, N.; Suzuki, K.; Masaki, Y.; et al. Ongoing hydrothermal activities within Enceladus. *Nature* **2015**, *519*, 207–210. [[CrossRef](#)] [[PubMed](#)]
10. Sekine, Y.; Shibuya, T.; Postberg, F.; Hsu, H.-W.; Suzuki, K.; Masaki, Y.; Kuwatani, T.; Mori, M.; Hong, P.K.; Yoshizaki, M.; Tachibana, S.; Sirono, S. High-temperature water–rock interactions and hydrothermal environments in the chondrite-like core of Enceladus. *Nat. Commun.* **2015**, *6*, 1–8. [[CrossRef](#)] [[PubMed](#)]
11. Jolliff, B.L. Fragments of quartz monzodiorite and felsite in Apollo 14 soil particles. In *Proceedings of the Twenty-First Lunar and Planetary Science Conference*, Houston, TX, USA, 12–16 March 1991; pp. 101–118.
12. Leroux, H.; Cordier, P. Magmatic cristobalite and quartz in the NWA 856 Martian meteorite. *Meteorit. Planet. Sci.* **2006**, *41*, 913–923. [[CrossRef](#)]
13. Akimoto, S.; Yagi, T.; Inoue, K. High temperature-pressure phase boundaries in silicate systems using in situ X-ray diffraction. In *High-Pressure Research, Applications in Geophysics*; Academic: New York, NY, USA, 1977; pp. 595–602.
14. Presnall, D.C. Phase diagrams of Earth-forming minerals. In *Mineral Physics & Crystallography: A Handbook of Physical Constants*; Ahrens, T.J., Ed.; American Geophysical Union: Washington, DC, USA, 1995; pp. 248–268.
15. Swamy, V.; Saxena, S.K.; Sundman, B.; Zhang, J. A thermodynamic assessment of silica phase diagram. *J. Geophys. Res.* **1994**, *99*, 11787–11794. [[CrossRef](#)]
16. Kuwayama, Y. Ultrahigh pressure and high temperature experiments using a laser heated diamond anvil cell in multimegabar pressures region. *Rev. High Press. Sci. Technol.* **2008**, *18*, 3–10. [[CrossRef](#)]

17. Tomioka, N.; Miyahara, M. High-pressure minerals in shocked meteorites. *Meteorit. Planet. Sci.* **2017**, *52*, 2017–2039. [[CrossRef](#)]
18. Kubo, T.; Kato, T.; Higo, Y.; Funakoshi, K. Curious kinetic behavior in silica polymorphs solves seifertite puzzle in shocked meteorite. *Sci. Adv.* **2015**, *1*, e1500075. [[CrossRef](#)] [[PubMed](#)]
19. Sharp, T.G.; El Goresy, A.; Wopenka, B.; Chen, M. A post-stishovite SiO₂ polymorph in the meteorite Shergotty: Implications for impact events. *Science* **1999**, *284*, 1511–1513. [[CrossRef](#)] [[PubMed](#)]
20. Kring, D.A.; Gleason, J.D. Magmatic temperatures and compositions on early Mars as inferred from the orthopyroxene-silica assemblage in ALH84001. In Proceedings of the Annual Meteoritical Society Meeting, Maui, HI, USA, 21–25 July 1997.
21. Pang, R.-L.; Zhang, A.-C.; Wang, S.-Z.; Wang, R.-C.; Yurimoto, H. High-pressure minerals in eucrite suggest a small source crater on Vesta. *Sci. Rep.* **2016**, *6*, 26063. [[CrossRef](#)] [[PubMed](#)]
22. Kihara, K. An X-ray study of the temperature dependence of the quartz structure. *Eur. J. Mineral.* **1990**, *2*, 63–78. [[CrossRef](#)]
23. Dollase, W.A.; Cliff, R.A.; Wetherill, G.W. Note on tridymite in rock 12021. *Proc. Lunar Sci. Conf.* **1971**, *1*, 141–142.
24. Konnert, J.H.; Appleman, D.E. The crystal structure of low tridymite. *Acta Cryst.* **1978**, *34*, 391–403. [[CrossRef](#)]
25. El Goresy, A.; Dera, P.; Sharp, T.G.; Prewitt, C.T.; Chen, M.; Dubrovinsky, L.; Wopenka, B.; Boctor, N.Z.; Hemley, R.J. Seifertite, a dense orthorhombic polymorph of silica from the Martian meteorites Shergotty and Zagami. *Eur. J. Mineral.* **2008**, *20*, 523–528. [[CrossRef](#)]
26. El Goresy, A.; Dubrovinsky, L.; Sharp, T.G.; Saxena, S.K.; Chen, M. A monoclinic post-stishovite polymorph of silica in the Shergotty meteorite. *Science* **2000**, *288*, 1632–1634. [[CrossRef](#)] [[PubMed](#)]
27. Papike, J.J.; Taylor, L.; Simon, S. Lunar minerals. In *Lunar Sourcebook*; Heiken, G.H., Vaniman, D.T., French, B.M., Eds.; Cambridge University Press: New York, NY, USA, 1991; pp. 121–181.
28. Warren, P.H. The magma ocean concept and lunar evolution. *Annu. Rev. Earth Planet. Sci.* **1985**, *13*, 201–240. [[CrossRef](#)]
29. Hiesinger, H.; Head, J.W.; Wolf, U.; Jaumann, R.; Neukum, G. Ages and stratigraphy of mare basalts in Oceanus Procellarum, Mare Nubium, Mare Cognitum, and Mare Insularum. *J. Geophys. Res.* **2003**, *108*, E001985. [[CrossRef](#)]
30. Morota, T.; Haruyama, J.; Ohtake, M.; Matsunaga, T.; Honda, C.; Yokota, Y.; Kimura, J.; Ogawa, Y.; Demura, H.; Iwasaki, A.; et al. Timing and characteristics of the latest mare eruption on the Moon. *Earth Planet. Sci. Lett.* **2011**, *302*, 255–266. [[CrossRef](#)]
31. Borg, L.E.; Gaffney, A.M.; Shearer, C.K.; DePaolo, D.J.; Hutcheon, I.D.; Owens, T.L.; Ramon, E.; Brennecka, G. Mechanisms for incompatible-element enrichment on the Moon deduced from the lunar basaltic meteorite Northwest Africa 032. *Geochim. Cosmochim. Acta* **2009**, *73*, 3963–3980. [[CrossRef](#)]
32. Jolliff, B.L.; Gillis, J.J.; Haskin, L.A.; Korotev, R.L.; Wieczorek, M.A. Major lunar crustal terranes: Surface expressions and crust-mantle origins. *J. Geophys. Res.* **2000**, *105*, 4197–4216. [[CrossRef](#)]
33. Ohtake, M.; Haruyama, J.; Matsunaga, T.; Yokota, Y.; Morota, T.; Honda, C.; LISM Team. Performance and scientific objectives of the SELENE (KAGUYA) Multiband Imager. *Earth Planets Space* **2008**, *60*, 257–264. [[CrossRef](#)]
34. Ohtake, M.; Matsunaga, T.; Haruyama, J.; Yokota, Y.; Morota, T.; Honda, C.; Ogawa, Y.; Torii, M.; Miyamoto, H.; Arai, T.; et al. The global distribution of pure anorthosite on the Moon. *Nature* **2009**, *461*, 236–240. [[CrossRef](#)] [[PubMed](#)]
35. Yamamoto, S.; Nakamura, R.; Matsunaga, T.; Ogawa, Y.; Ishihara, Y.; Morota, T.; Hirata, N.; Ohtake, M.; Hiroi, T.; Yokota, Y.; et al. Possible mantle origin of olivine around lunar impact basins detected by SELENE. *Nat. Geosci.* **2010**, *3*, 533–536. [[CrossRef](#)]
36. Neal, C.R.; Taylor, T.A. Petrogenesis of mare basalts: A record of lunar volcanism. *Geochim. Cosmochim. Acta* **1992**, *56*, 2177–2211. [[CrossRef](#)]
37. Taylor, G.J.; Warren, P.H.; Ryder, G.; Delano, J.; Pieters, C.; Lofgren, G. Lunar rocks. In *Lunar Sourcebook*; Heiken, G.H., Vaniman, D.T., French, B.M., Eds.; Cambridge University Press: New York, NY, USA, 1991; pp. 183–284.
38. Neal, C.R. The Moon 35 years after Apollo: What's left to learn? *Chem. Erde-Geochem.* **2008**. [[CrossRef](#)]
39. Ryder, G. Lunar sample 15405: Remnant of a KREEP basalt-granite differentiated pluton. *Earth Planet. Sci. Lett.* **1976**, *29*, 255–268. [[CrossRef](#)]

40. Seddio, S.M.; Korotev, R.L.; Jolliff, B.L.; Wang, A. Silica polymorphs in lunar granite: Implications for granite petrogenesis on the Moon. *Am. Mineral.* **2015**, *100*, 1533–1543. [[CrossRef](#)]
41. Seddio, S.M.; Jolliff, B.L.; Korotev, R.L.; Carpenter, P.K. Thorite in an Apollo 12 granite fragment and age determination using the electron microprobe. *Geochim. Cosmochim. Acta* **2014**, *135*, 307–320. [[CrossRef](#)]
42. Meyer, C.; Williams, I.S.; Compston, W. Uranium-lead ages for lunar zircons: Evidence for a prolonged period of granophyre formation from 4.32 to 3.88 Ga. *Meteorit. Planet. Sci.* **1996**, *31*, 370–387. [[CrossRef](#)]
43. Warren, P.H.; Kallemeyn, G.W. Geochemical investigations of five lunar meteorites: Implications for the composition, origin and evolution of the lunar crust. *Antarct. Meteor. Res.* **1991**, *4*, 91–117.
44. Arai, T.; Takeda, H.; Yamaguchi, A.; Ohtake, M. A new model of lunar crust: Asymmetry in crustal composition and evolution. *Earth Planet. Space* **2008**, *60*, 433–444. [[CrossRef](#)]
45. Gross, J.; Treiman, A.H.; Mercer, C.N. Lunar feldspathic meteorites: Constraints on the geology of the lunar highlands, and the origin of the lunar crust. *Earth Planet. Sci. Lett.* **2014**, *388*, 318–328. [[CrossRef](#)]
46. Korotev, R.L. Lunar geochemistry as told by lunar meteorites. *Chem. Erde-Geochem.* **2005**, *65*, 297–346. [[CrossRef](#)]
47. Korotev, R.L.; Jolliff, B.L.; Zeigler, R.A.; Gillis, J.J.; Haskin, L.A. Feldspathic lunar meteorites and their implications for compositional remote sensing of the lunar surface and the composition of the lunar crust. *Geochim. Cosmochim. Acta* **2003**, *67*, 4895–4923. [[CrossRef](#)]
48. Nagaoka, H.; Takeda, H.; Karouji, Y.; Ohtake, M.; Yamaguchi, A.; Yoneda, S.; Hasebe, N. Implications for the origins of pure anorthosites found in the feldspathic lunar meteorites, Dhofar 489 group. *Earth Planets Space* **2014**, *66*, 115. [[CrossRef](#)]
49. Takeda, H.; Yamaguchi, A.; Bogard, D.D.; Karouji, Y.; Ebihara, M.; Ohtake, M.; Saiki, K.; Arai, T. Magnesian anorthosites and a deep crustal rock from the farside crust of the moon. *Earth Planet. Sci. Lett.* **2006**, *247*, 171–184. [[CrossRef](#)]
50. Treiman, A.H.; Maloy, A.K.; Shearer, C.K., Jr.; Gross, J. Magnesian anorthositic granulites in lunar meteorites Allan Hills A81005 and Dhofar 309: Geochemistry and global significance. *Meteorit. Planet. Sci.* **2010**, *45*, 163–180. [[CrossRef](#)]
51. Warren, P.H.; Ulff-Møller, F.; Kallemeyn, G.W. ‘New’ lunar meteorites: Impact melt and regolith breccias and large-scale heterogeneities of the upper lunar crust. *Meteorit. Planet. Sci.* **2005**, *40*, 989–1014. [[CrossRef](#)]
52. Yamaguchi, A.; Karouji, Y.; Takeda, H.; Nyquist, L.E.; Bogard, D.D.; Ebihara, M.; Shih, C.-Y.; Reese, Y.D.; Garrison, D.; Park, J.; et al. The variety of lithologies in the Yamato-86032 lunar meteorite: Implications for formation processes of the lunar crust. *Geochim. Cosmochim. Acta* **2010**, *74*, 4507–4530. [[CrossRef](#)]
53. List of Lunar Meteorites. Available online: http://meteorites.wustl.edu/moon_meteorites_list_alumina.htm (accessed on 9 April 2018).
54. Jolliff, B.L.; Korotev, R.L.; Zeigler, R.A.; Floss, C. Northwest Africa 773: Lunar mare breccia with a shallow-formed olivine-cumulate component, inferred very-low-Ti (VLT) heritage, and a KREEP connection. *Geochim. Cosmochim. Acta* **2003**, *67*, 4857–4879. [[CrossRef](#)]
55. Fagan, T.J.; Taylor, G.J.; Keil, K.; Hicks, T.L.; Killgore, M.; Bunch, T.E.; Wittke, J.H.; Mittlefehldt, D.W.; Clayton, R.N.; Mayeda, T.K.; et al. Northwest Africa 773: Lunar origin and iron-enrichment trend. *Meteorit. Planet. Sci.* **2003**, *38*, 529–554. [[CrossRef](#)]
56. Fagan, T.J.; Kashima, D.; Wakabayashi, Y.; Suginoara, A. Case study of magmatic differentiation trends on the Moon based on lunar meteorite Northwest Africa 773 and comparison with Apollo 15 quartz monzodiorite. *Geochim. Cosmochim. Acta* **2014**, *133*, 97–127. [[CrossRef](#)]
57. Zhang, A.-C.; Hsu, W.-B.; Floss, C.; Li, X.-H.; Li, Q.-L.; Liu, Y.; Taylor, L.A. Petrogenesis of lunar meteorite Northwest Africa 2977: Constraints from in situ microprobe results. *Meteorit. Planet. Sci.* **2011**, *45*, 1929–1947. [[CrossRef](#)]
58. Collins, S.J.; Righter, K.; Brandon, A. Mineralogy, petrology and oxygen fugacity of the LaPaz Ice Field lunar basaltic meteorites and the origin and evolution of evolved lunar basalts. In Proceedings of the Thirty-Sixth Lunar and Planetary Science Conference, League City, TX, USA, 14–18 March 2005.
59. Wang, Y.; Hsu, W.; Guan, Y.; Li, X.; Li, Q.; Liu, Y.; Tang, G. Petrogenesis of the Northwest Africa 4734 basaltic lunar meteorite. *Geochim. Cosmochim. Acta* **2012**, *92*, 329–344. [[CrossRef](#)]
60. Al-Kathiri, A.; Gnos, E.; Hofmann, B.A. The regolith portion of the lunar meteorite Sayh al Uhaymir 169. *Meteorit. Planet. Sci.* **2007**, *42*, 2137–2152. [[CrossRef](#)]

61. Ashley, J.M.; Robinson, M.S.; Stopar, J.D.; Glotch, T.D.; Hawke, B.R.; van der Bogert, C.H.; Hiesinger, H.; Lawrence, S.J.; Jolliff, B.L.; Greenhagen, B.T.; et al. The Lassell massif-A silicic lunar volcano. *Icarus* **2016**, *273*, 248–261. [[CrossRef](#)]
62. Glotch, T.D.; Lucey, P.G.; Bandfield, J.L.; Greenhagen, B.T.; Thomas, I.R.; Elphic, R.C.; Bowles, N.; Wyatt, M.B.; Allen, C.C.; Hanna, K.D.; et al. Highly silicic compositions on the Moon. *Science* **2010**, *329*, 1510–1513. [[CrossRef](#)] [[PubMed](#)]
63. Hagerty, J.J.; Lawrence, D.J.; Hawke, B.R.; Vaniman, D.T.; Elphic, R.C.; Feldman, W.C. Refined thorium abundances for lunar red spots: Implications for evolved, nonmare volcanism on the Moon. *J. Geophys. Res.* **2006**, *111*, E06002. [[CrossRef](#)]
64. Jolliff, B.L.; Wiseman, S.A.; Lawrence, S.J.; Tran, T.N.; Robinson, M.S.; Sato, H.; Hawke, B.R.; Scholten, F.; Oberst, J.; Hiesinger, H.; et al. Non-mare silicic volcanism on the lunar farside at Compton-Belkovich. *Nat. Geosci.* **2011**, *4*, 566–571. [[CrossRef](#)]
65. Wilson, J.T.; Eke, V.R.; Massey, R.J.; Elphic, R.C.; Jolliff, B.L.; Lawrence, D.L.; Llewellyn, E.W.; McElwaine, J.N.; Teodoro, L.F.A. Evidence for explosive silicic volcanism on the Moon from the extended distribution of thorium near the Compton-Belkovich Volcanic Complex. *J. Geophys. Res.* **2015**, *120*, 92–108. [[CrossRef](#)]
66. Roedder, E.; Weiblen, P.W. Lunar petrology of silicate melt inclusions, Apollo 11 rocks. *Geochim. Cosmochim. Acta Suppl.* **1970**, *1*, 801–837.
67. Sharp, T.G.; DeCarli, P.S. Shock effects in meteorites. In *Meteorites and the Early Solar System*; Lauretta, D.S., McSween, H.Y., Eds.; Arizona University Press: Tucson, AZ, USA, 2006; pp. 653–678.
68. Biren, M.B.; Spray, J.G. Shock veins in the central uplift of the Manicouagan impact structure: Context and genesis. *Earth Planet. Sci. Lett.* **2011**, *303*, 310–322. [[CrossRef](#)]
69. Koeberl, C.; Kurat, G.; Brandstätter, F. Gabbroic lunar mare meteorites Asuka-881757 (Asuka-31) and Yamato 793169: Geochemical and mineralogical study. *Antarct. Meteor. Res.* **1993**, *6*, 14–34.
70. Arai, T.; Takeda, H.; Warren, P.H. Four lunar meteorites: Crystallization trends of pyroxenes and spinels. *Meteorit. Planet. Sci.* **1996**, *31*, 877–892. [[CrossRef](#)]
71. El Goresy, A.; Gillet, P.; Chen, M.; Stähle, V.; Graup, G. In situ finding of the fabric settings of shock-induced quartz/coesite phase transition in crystalline clasts in suevite of the Ries crater, Germany. In Proceedings of the 64th Annual Meteoritical Society Meeting, Vatican City, Italy, 10–14 September 2001.
72. Ling, Z.C.; Wang, A.; Jolliff, B.L. Mineralogy and geochemistry of four lunar soils by laser-Raman study. *Icarus* **2011**, *211*, 101–113. [[CrossRef](#)]
73. Misawa, K.; Tatsumoto, M.; Dalrymple, G.B.; Yanai, K. An extremely low U/Pb source in the Moon: U-Th-Pb, Sm-Nd, Rb-Sr, and $^{40}\text{Ar}/^{39}\text{Ar}$ isotopic systematics and age of lunar meteorite Asuka 881757. *Geochim. Cosmochim. Acta* **1993**, *57*, 4687–4702. [[CrossRef](#)]
74. Hiesinger, H.; Head, J.W., III. New Views of Lunar Geoscience: An Introduction and Overview. In *New Views of the Moon, Reviews in Mineralogy & Geochemistry*; Jolliff, B.L., Wiczorek, M.A., Shearer, C.K., Neal, C.R., Eds.; Mineralogical Society of America: Chantilly, VA, USA, 2006; Volume 60, pp. 1–81.
75. Nishiizumi, K.; Arnold, J.R.; Caffee, M.W.; Finkel, R.C.; Southon, J. Cosmic ray exposure histories of lunar meteorites Asuka 881757, Yamato 793169, and Calalong Creek. In Proceedings of the 17th Symposium on Antarctic Meteorites, Tokyo, Japan, 19–21 August 1992; pp. 129–132.
76. Hemley, R.J.; Prewitt, C.T.; Kingma, K.J. High-pressure behavior of silica. *Rev. Mineral.* **1994**, *29*, 41–81.
77. Murakami, M.; Hirose, K.; Ono, S.; Ohishi, Y. Stability of CaCl_2 -type and $\alpha\text{-PbO}_2$ at high pressure and temperature determined by in-situ X-ray measurements. *Geophys. Res. Lett.* **2003**, *30*, 1207. [[CrossRef](#)]
78. Kuwayama, Y.; Hirose, K.; Sata, N.; Ohishi, Y. The pyrite-type high-pressure form of silica. *Science* **2005**, *309*, 923–925. [[CrossRef](#)] [[PubMed](#)]
79. Tsuchida, Y.; Yagi, T. New pressure-induced transformations of silica at room temperature. *Nature* **1990**, *347*, 267–269. [[CrossRef](#)]
80. Dubrovinsky, L.S.; Saxena, S.K.; Lazor, P.; Ahuja, R.; Eriksson, O.; Wills, J.M.; Johansson, B. Pressure-induced transformations of cristobalite. *Chem. Phys. Lett.* **2001**, *333*, 264–270. [[CrossRef](#)]
81. Melosh, H.J. A Geologic Process. In *Impact Cratering*; Oxford University Press: New York, NY, USA, 1989.
82. Blaß, U.W. Shock-induced formation mechanism of seifertite in shergottites. *Phys. Chem. Miner.* **2013**, *40*, 425–437. [[CrossRef](#)]

83. Marchi, S.; Bottke, W.F.; Cohen, B.A.; Wuennemann, K.; Kring, D.A.; McSween, H.Y.; De Sanctis, M.C.; O'Brien, D.P.; Schenk, P.; Raymond, C.A.; et al. High-velocity collisions from the lunar cataclysm recorded in asteroidal meteorites. *Nat. Geosci.* **2013**, *6*, 303–307. [[CrossRef](#)]
84. Taylor, S.R.; Gorton, M.P.; Muir, P.; Nance, W.; Rudowski, R.; Ware, N. Lunar highlands composition: Apennine Front. *Geochim. Cosmochim. Acta* **1973**, *2*, 1445–1459.
85. McKay, D.S.; Bogard, D.D.; Morris, R.V.; Korotev, R.L.; Wentworth, S.J.; Johnson, P. Apollo 15 regolith breccias: Window to a KREEP regolith. In Proceedings of the 19th Lunar and Planetary Science Conference, Houston, TX, USA, 14–19 March 1989; pp. 19–41.
86. Langenhorst, F.; Poirier, J.P. “Eclogitic” minerals in a shocked basaltic meteorite. *Earth Planet. Sci. Lett.* **2000**, *176*, 259–265. [[CrossRef](#)]
87. Langenhorst, F.; Poirier, J.P. Anatomy of black veins in Zagami: Clues to the formation of high-pressure phases. *Earth Planet. Sci. Lett.* **2000**, *184*, 37–55. [[CrossRef](#)]
88. Beck, P.; Gillet, P.; Gautron, L.; Daniel, I.; El Goresy, A. A new natural high-pressure (Na, Ca)-hexaluminosilicate $[(Ca_xNa_{1-x})Al_{3+x}Si_{3-x}O_{11}]$ in shocked Martian meteorites. *Earth Planet. Sci. Lett.* **2004**, *219*, 1–12. [[CrossRef](#)]
89. Miyahara, M.; Ohtani, E.; Yamaguchi, A.; Ozawa, S.; Sakai, T.; Hirao, N. Discovery of coesite and stishovite in eucrite. *Proc. Natl. Acad. Sci. USA* **2014**, *111*, 10939–10942. [[CrossRef](#)] [[PubMed](#)]
90. Akaogi, M.; Navrotsky, A. The quartz–coesite–stishovite transformations: New calorimetric measurements and calculation of phase diagrams. *Phys. Earth Planet. Inter.* **1984**, *36*, 124–134. [[CrossRef](#)]
91. Zhang, J.; Liebermann, R.C.; Gasparik, T.; Herzberg, C.T.; Fei, Y. Melting and subsolidus relations of SiO₂ at 9–14 GPa. *J. Geophys. Res.* **1993**, *98*, 19785–19793. [[CrossRef](#)]
92. Duke, M.B.; Gaddis, L.R.; Taylor, G.J.; Schmitt, H.H. Earth-Moon System, Planetary Science, and Lessons Learned. In *New Views of the Moon, Reviews in Mineralogy & Geochemistry*; Jolliff, B.L., Wiczorek, M.A., Shearer, C.K., Neal, C.R., Eds.; Mineralogical Society of America: Chantilly, VA, USA, 2006; pp. 657–704.
93. Sunshine, J.M.; Farnham, T.L.; Feaga, L.M.; Groussin, O.; Merlin, F.; Milliken, R.E.; A'Hearn, M.F. Temporal and spatial variability of lunar hydration as observed by the deep impact spacecraft. *Science* **2009**, *326*, 565–568. [[CrossRef](#)] [[PubMed](#)]
94. Colaprete, A.; Schultz, P.; Heldmann, J.; Wooden, D.; Shirley, M.; Ennico, K.; Hermalyn, B.; Marshall, W.; Ricco, A.; Elphic, R.C.; et al. Detection of water in the LCROSS ejecta plume. *Science* **2010**, *330*, 463–468. [[CrossRef](#)] [[PubMed](#)]
95. Schäf, O.; Ghobarkar, H.; Garnier, A.; Vagner, C.; Lindner, J.K.N.; Hanss, J.; Reller, A. Synthesis of nanocrystalline low temperature silica polymorphs. *Solid State Sci.* **2006**, *8*, 625–633. [[CrossRef](#)]
96. Kyono, A.; Yokooji, M.; Chiba, T.; Tamura, T.; Tuji, A. Pressure-induced crystallization of biogenic hydrous amorphous silica. *J. Mineral. Petrol. Sci.* **2017**, *112*, 324–335. [[CrossRef](#)]
97. Heaney, P.J.; Post, J.E. The widespread distribution of a novel silica polymorph in microcrystalline quartz varieties. *Science* **1992**, *255*, 441–443. [[CrossRef](#)] [[PubMed](#)]
98. Heaney, P.J. Moganite as an indicator for vanished evaporites: A testament reborn? *J. Sediment. Res.* **1995**, *65*, 633–638.
99. Petrovic, I.; Heaney, P.J.; Navrotsky, A. Thermochemistry of the new silica polymorph moganite. *Phys. Chem. Miner.* **1996**, *23*, 119–126. [[CrossRef](#)]
100. Götze, J.; Nasdala, L.; Kleeberg, R.; Wenzel, M. Occurrence and distribution of “moganite” in agate/chalcedony: A combined micro-Raman, Rietveld, and cathodoluminescence study. *Contrib. Mineral. Petrol.* **1998**, *133*, 96–105. [[CrossRef](#)]
101. Fernandes, V.A.; Burgess, R.; Turner, G. ⁴⁰Ar–³⁹Ar chronology of lunar meteorites Northwest Africa 032 and 773. *Meteorit. Planet. Sci.* **2003**, *38*, 555–564. [[CrossRef](#)]
102. Nishiizumi, K.; Hillegonds, D.J.; McHargue, L.R.; Jull, A.J.T. Exposure and terrestrial histories of new lunar and martian meteorites. In Proceedings of the 35th Lunar and Planetary Science Conference, League City, TX, USA, 15–19 March 2004.
103. Schorghofer, N.; Taylor, G.J. Subsurface migration of H₂O at lunar cold traps. *J. Geophys. Res.* **2007**, *112*, E02010. [[CrossRef](#)]
104. Zuber, M.T.; Head, J.W.; Smith, D.E.; Neumann, G.A.; Mazarico, E.; Torrence, M.H.; Aharonson, O.; Tye, A.R.; Fassett, C.I.; Rosenburg, M.A.; et al. Constraints on the volatile distribution within Shackleton crater at the lunar south pole. *Nature* **2012**, *486*, 378–381. [[CrossRef](#)] [[PubMed](#)]

105. Meteoritical Bulletin Database. Available online: <https://www.lpi.usra.edu/meteor/> (accessed on 15 June 2018).
106. Nyquist, L.E.; Bogard, D.D.; Shih, C.-Y.; Greshake, A.; Stoffler, D.; Eugster, O. Ages and geologic histories of Martian meteorites. *Chronol. Evol. Mars* **2001**, *96*, 105–164.
107. Niihara, T. Uranium-lead age of baddeleyite in shergottite Roberts Massif 04261: Implications for magmatic activity on Mars. *J. Geophys. Res.* **2011**, *116*, E12008. [[CrossRef](#)]
108. Fritz, J.; Artemieva, N.; Greshake, A. Ejection of Martian meteorites. *Meteorit. Planet. Sci.* **2005**, *40*, 1393–1411. [[CrossRef](#)]
109. Mittlefehldt, D.W. ALH84001, a cumulate orthopyroxenite member of the Martian meteorite clan. *Meteoritics* **1994**, *29*, 214–221. [[CrossRef](#)]
110. Romanek, C.S.; Grady, M.M.; Wright, I.P.; Mittlefehldt, D.W.; Socki, R.A.; Pillinger, C.T.; Gibson, E.K. Record of fluid-rock interactions on Mars from the meteorite ALH84001. *Nature* **1994**, *372*, 655–657. [[CrossRef](#)] [[PubMed](#)]
111. Romanek, C.S.; Thomas, K.L.; Gibson, E.K.; McKay, D.S.; Socki, R.A. Carbon and sulfur-bearing minerals in the Martian meteorite Allan Hills 84001. *Meteoritics* **1995**, *30*, 567–568.
112. Dreibus, G.; Burghelle, A.; Jochum, K.P.; Spettel, B.; Wlotzka, F.; Wänke, H. Chemical and mineral composition of ALH84001: A Martian orthopyroxenite. *Meteoritics* **1994**, *29*, 461.
113. Harvey, R.P.; McSween, H.Y. A possible high-temperature origin for the carbonates in Martian meteorite ALH84001. *Nature* **1996**, *382*, 49–51. [[CrossRef](#)] [[PubMed](#)]
114. McKay, D.S.; Gibson, E.K.; Thomas-Keprta, K.L.; Vali, H.; Romanek, C.S.; Clemett, S.J.; Chillier, X.D.F.; Maechling, C.R.; Zare, R.N. Search for life on Mars: Possible relic biogenic activity in Martian meteorite ALH84001. *Science* **1996**, *273*, 924–930. [[CrossRef](#)] [[PubMed](#)]
115. McKay, D.S.; Thomas-Keprta, K.L.; Romanek, C.S.; Gibson, E.K.; Vali, H. Evaluating the evidence for past life on Mars: Response. *Science* **1996**, *274*, 2123–2124.
116. Corrigan, C.M.; Harvey, R.P.; Bradley, J. Sodium-bearing pyroxene in ALH 84001. In Proceedings of the Thirty-First Lunar and Planetary Science Conference, Houston, TX, USA, 13–17 March 2000; p. 1762.
117. Corrigan, C.M.; Harvey, R.P. Multi-generational carbonate assemblages in martian meteorite Allan Hills 84001: Implications for nucleation, growth and alteration. *Meteorit. Planet. Sci.* **2004**, *39*, 17–30. [[CrossRef](#)]
118. Brearley, A.J. Hydrous phases in ALH84001: Further evidence for preterrestrial alteration and a shock-induced thermal overprint. In Proceedings of the Thirty-First Lunar and Planetary Science Conference, Houston, TX, USA, 13–17 March 2000.
119. Greenwood, J.O.; McSween, H.Y., Jr. Petrogenesis of Allan Hills 84001: Constraints from impact-melted feldspathic and silica glasses. *Meteorit. Planet. Sci.* **2001**, *36*, 43–61. [[CrossRef](#)]
120. Melwani Daswani, M.; Schwenzer, S.P.; Reed, M.H.; Wright, I.P.; Grady, M.M. Alteration minerals, fluids, and gases on early Mars: Predictions from 1-D flow geochemical modeling of mineral assemblages in meteorite ALH 84001. *Meteorit. Planet. Sci.* **2016**, *51*, 2154–2174. [[CrossRef](#)]
121. Scott, E.R.D.; Yamaguchi, A.; Krot, A.N. Petrological evidence for shock melting of carbonates in the Martian meteorite ALH84001. *Nature* **1997**, *387*, 377–379. [[CrossRef](#)] [[PubMed](#)]
122. Turner, G.; Knott, S.F.; Ash, R.D.; Gilmour, J.D. Ar-Ar chronology of the Martian meteorite ALH84001: Evidence for the timing of the early bombardment of Mars. *Geochim. Cosmochim. Acta* **1997**, *61*, 3835–3850. [[CrossRef](#)]
123. Valley, J.W.; Eiler, J.M.; Graham, C.M.; Gibson, E.K.; Romanek, C.S.; Stolper, E.M. Low-temperature carbonate concretions in the Martian meteorite ALH84001: Evidence from stable isotopes and mineralogy. *Science* **1997**, *275*, 1633–1637. [[CrossRef](#)] [[PubMed](#)]
124. Cooney, T.F.; Scott, E.R.D.; Krot, A.N.; Sharma, S.K.; Yamaguchi, A. Vibrational spectroscopic study of minerals in the Martian meteorite ALH84001. *Am. Mineral.* **1999**, *84*, 1569–1576. [[CrossRef](#)]
125. White, L.M.; Gibson, E.K.; Thomas-Keprta, K.L.; Clemett, S.J.; McKay, D.S. Putative indigenous carbon-bearing-alteration features in Martian meteorite Yamato 000593. *Astrobiology* **2014**, *14*, 170–181. [[CrossRef](#)] [[PubMed](#)]
126. Imae, N.; Ikeda, Y.; Shinoda, K.; Kojima, H.; Iwata, N. Yamato Nakhilites: Petrography and mineralogy. *Antarct. Meteor. Res.* **2003**, *16*, 13–33.
127. Symes, S.J.; Borg, L.E.; Shearer, C.K.; Irving, A.J. The age of the Martian meteorite Northwest Africa 1195 and the differentiation history of the Shergottites. *Geochim. Cosmochim. Acta* **2008**, *72*, 1696–1710. [[CrossRef](#)]

128. Herd, C.D.K.; Walton, E.L.; Agee, C.B.; Muttik, N.; Ziegler, K.; Shearer, C.K.; Bell, A.S.; Santos, A.R.; Burger, P.V.; Simon, J.I.; et al. The Northwest Africa 8159 martian meteorite: Expanding the martian meteorite suite to the Amazonian. *Geochim. Cosmochim. Acta* **2017**, *218*, 1–26. [[CrossRef](#)]
129. Smith, J.V.; Hervig, R.L. Shergotty meteorite: Mineralogy, petrography, and minor elements. *Meteoritics* **1979**, *14*, 121–142. [[CrossRef](#)]
130. McSween, H.Y.; Taylor, L.A.; Stolper, E.M. Allan Hills 77005: A new meteorite type found in Antarctica. *Science* **1979**, *204*, 1201–1203. [[CrossRef](#)] [[PubMed](#)]
131. Ikeda, Y. Petrology of magmatic silicate inclusions in the Allan Hills 77005 Lherzolithic Shergottite. *Meteorit. Planet. Sci.* **1998**, *33*, 803–812. [[CrossRef](#)]
132. Malavergne, V.; Guyot, F.; Benzerara, K.; Martinez, I. Description of new shock-induced phases in the Shergotty, Zagami, Nakhla and Chassigny meteorites. *Meteorit. Planet. Sci.* **2001**, *36*, 1297–1305. [[CrossRef](#)]
133. Barrat, J.A.; Gillet, P.; Sautter, V.; Jambon, A.; Javoy, M.; Göpel, C.; Lesourd, M.; Keller, F.; Petit, E. Petrology and geochemistry of the basaltic Shergottite Northwest Africa 480. *Meteorit. Planet. Sci.* **2002**, *37*, 487–499. [[CrossRef](#)]
134. Jambon, A.; Barrat, J.-A.; Sautter, V.; Gillet, P.; Göpel, C.; Javoy, M.; Joron, J.-L.; Lesourd, M. The basaltic Shergottite Northwest Africa 856: Petrology and chemistry. *Meteorit. Planet. Sci.* **2002**, *37*, 1147–1164. [[CrossRef](#)]
135. Taylor, L.A.; Nazarov, M.A.; Shearer, C.K.; McSween, H.Y., Jr.; Cahill, J.; Neal, C.R.; Icanova, M.A.; Barsukova, L.D.; Lentz, R.C.; Clayton, R.N.; et al. Martian meteorite Dhofar 019: A new Shergottite. *Meteorit. Planet. Sci.* **2002**, *37*, 1107–1128. [[CrossRef](#)]
136. Mikouchi, T.; Barrat, J.A. NWA 5029 Basaltic Shergottite: A Clone of NWA 480/1460? In Proceedings of the 72nd Annual Meeting of the Meteoritical Society, Nancy, France, 13–18 July 2009.
137. Howarth, G.H.; Udry, A.; Day, J.M.D. Petrogenesis of basaltic shergottite Northwest Africa 8657: Implications for fO₂ correlations and element redistribution during shock melting in shergottites. *Meteorit. Planet. Sci.* **2018**, *53*, 249–267. [[CrossRef](#)]
138. Irving, A.J.; Kuehner, S.M. Northwest Africa 5298: A strongly shocked basaltic Shergottite equilibrated at QFM and high temperature. *Meteorit. Planet. Sci.* **2008**, *43*, A63.
139. Hui, H.; Peslier, A.; Lapan, T.; Schafer, J.; Brandon, A.; Irving, A.J. Petrogenesis of basaltic Shergottite Northwest Africa 5298: Closed system crystallization of an oxidized mafic melt. *Meteorit. Planet. Sci.* **2011**, *46*, 1313–1328. [[CrossRef](#)]
140. Mikouchi, T. Mineralogical similarities and differences between the Los Angeles basaltic shergottite and the Asuka-881757 lunar mare meteorite. *Antarct. Meteor. Res.* **2001**, *14*, 1–20.
141. Chennaoui Aoudjehane, H.; Jambon, A.; Reynard, B.; Blanc, P. Silica as a shock index in Shergottites: A catholuminescence study. *Meteorit. Planet. Sci.* **2005**, *40*, 1–14.
142. Stöffler, D.; Ostertag, R.; Jammes, C.; Pfannschmidt, G.; Sen Gupta, P.R.; Simon, S.B.; Papike, J.J.; Beauchamp, R.H. Shock metamorphism and petrography of the Shergotty achondrite. *Geochim. Cosmochim. Acta* **1986**, *50*, 889–913. [[CrossRef](#)]
143. El Goresy, A.; Gillet, P.; Miyahara, M.; Ohtani, E.; Ozawa, S.; Beck, P.; Montagnac, G. Shock-induced deformation of Shergottites: Shock–pressures and perturbations of magmatic ages on Mars. *Geochim. Cosmochim. Acta* **2013**, *101*, 233–262. [[CrossRef](#)]
144. Ikeda, Y.; Kimura, M.; Takeda, H.; Shimoda, G.; Kita, N.T.; Morishita, Y.; Suzuki, A.; Jagoutz, E.; Dreibus, G. Petrology of a new basaltic Shergottite: Dhofar 378. *Antarct. Meteor. Res.* **2006**, *19*, 20–44.
145. Hu, S.; Lin, Y.T.; Zhang, T.; Gu, L.X.; Tang, X. Discovery of first coesite in the martian meteorite Northwest Africa 8675. In Proceedings of the 80th Annual Meeting of the Meteoritical Society, Santa Fe, NM, USA, 23–28 July 2017.
146. McCoy, T.J.; Lofgren, G.E. Crystallization of the Zagami Shergottite: An experimental study. *Earth Planet. Sci. Lett.* **1999**, *173*, 397–411. [[CrossRef](#)]
147. Niihara, T.; Misawa, K.; Mikouchi, T.; Nyquist, L.E.; Park, J.; Yamashita, H.; Hirata, D. Complex formation history of highly evolved basaltic shergottite, Zagami. In Proceedings of the 75th Annual Meeting of the Meteoritical Society, Cairns, Australia, 12–17 August 2012.
148. Rubin, A.E.; Warren, P.H.; Greenwood, J.P.; Verish, R.S.; Leshin, L.A.; Hervig, R.L.; Clayton, R.N.; Mayeda, T.K. Los Angeles: The most differentiated basaltic Martian meteorite. *Geology* **2000**, *28*, 1011–1014. [[CrossRef](#)]

149. Warren, P.H.; Greenwood, J.P.; Rubin, A.E. Los Angeles: A tale of two stones. *Meteorit. Planet. Sci.* **2004**, *39*, 137–156. [[CrossRef](#)]
150. Rost, D.; Stephan, T.; Geshake, A.; Fritz, J.; Jesseberger, E.K.; Weber, I.; Stoffler, D. A combined TOF-SIMS, EMP/SEM of a three-phase symplectite in the Los Angeles basaltic Shergottite. *Meteorit. Planet. Sci.* **2009**, *44*, 1225–1237. [[CrossRef](#)]
151. Aramovich, C.J.; Herd, C.D.K.; Papike, J.J. Symplectites derived from metastable phases in Martian basaltic meteorites. *Am. Mineral.* **2002**, *87*, 1351–1359. [[CrossRef](#)]
152. Roszjar, J.; Bishoff, A.; Llorca, J.; Pack, A. Ksar Gilane 002 (KG002)—A new Shergottite: Discovery, mineralogy, chemistry and oxygen isotopes. In Proceedings of the 43rd Lunar and Planetary Science Conference, The Woodlands, TX, USA, 19–23 March 2012.
153. Llorca, J.; Roszjar, J.; Cartwright, J.A.; Bischoff, A.; Ott, U.; Pack, A.; Merchel, S.; Rugel, G.; Fimiani, L.; Ludwig, P.; et al. The Ksar Ghilane 002 shergottite—The 100th registered Martian meteorite fragment. *Meteorit. Planet. Sci.* **2013**, *48*, 493–513. [[CrossRef](#)]
154. Bunch, T.E.; Irving, A.J.; Wittke, J.H.; Kuehner, S.M. Highly evolved basaltic Shergottite Northwest Africa 2800: A clone of Los Angeles. In Proceedings of the Thirty-Ninth Lunar and Planetary Science Conference, League City, TX, USA, 10–14 March 2008.
155. Udry, A.; Howarth, G.H.; Lapen, T.J.; Righter, M. Petrogenesis of the NWA 7320 enriched martian gabbroic shergottite: Insight into the martian crust. *Geochim. Cosmochim. Acta* **2017**, *204*, 1–18. [[CrossRef](#)]
156. Lindsley, D.H. Pyroxene thermometry. *Am. Mineral.* **1983**, *68*, 477–493.
157. Agee, C.B.; Wilson, N.V.; McCubbin, F.M.; Ziegler, K.; Polyak, V.J.; Sharp, Z.D.; Asmerom, Y.; Nunn, M.H.; Shaheen, R.; Thiemens, M.H.; et al. Unique meteorite from early Amazonian Mars: Water-rich basaltic breccia Northwest Africa 7034. *Science* **2013**, *339*, 780–785. [[CrossRef](#)] [[PubMed](#)]
158. Beck, P.; Pommerol, A.; Zanda, B.; Remusat, L.; Lorand, J.P.; Göpel, C.; Hewins, R.; Pont, S.; Lewin, E.; Quirico, E.; et al. A Noachian source region for the “Black Beauty” meteorite, and a source lithology for Mars surface hydrated dust? *Earth Planet. Sci. Lett.* **2015**, *427*, 104–111. [[CrossRef](#)]
159. Ruff, S.W.; Farmer, J.D. Silica deposits in Mars with features resembling hot spring biosignatures at El Tatio in Chile. *Nat. Commun.* **2016**, *7*, 13554. [[CrossRef](#)] [[PubMed](#)]
160. Morris, R.V.; Vaniman, D.T.; Blake, D.F.; Gellert, R.; Chipera, S.J.; Rampe, E.B.; Ming, D.W.; Morrison, S.M.; Downs, R.T.; Treimann, A.H.; et al. Silicic volcanism on Mars evidenced by tridymite in high-SiO₂ sedimentary rock at Gale crater. *Proc. Natl. Acad. Sci. USA* **2016**, *113*, 7071–7076. [[CrossRef](#)] [[PubMed](#)]
161. Ma, C.; Tschauer, O.; Becett, J.R.; Liu, Y.; Rossman, G.R.; Zhuravlev, K.; Prakapenka, V.; Dera, P.; Taylor, L.A. Tissintite, (Ca, Na, □)AlSi₂O₆, a highly-defective, shock-induced, high-pressure clinopyroxene in the Tissint martian meteorite. *Earth Planet. Sci. Lett.* **2015**, *422*, 194–205. [[CrossRef](#)]
162. Teter, D.M.; Hemley, R.J.; Kresse, G.; Hafner, J. High pressure polymorphism in silica. *Phys. Rev. Lett.* **1998**, *80*, 2145–2148. [[CrossRef](#)]
163. Kingma, K.; Cohen, R.E.; Hemley, R.J.; Mao, H.-K. Transformation of stishovite to a denser phase at lower-mantle pressures. *Nature* **1995**, *374*, 243–245. [[CrossRef](#)]
164. Dubrovinsky, L.S.; Saxena, S.K.; Lazor, P.; Ahuja, R.; Eriksson, O.; Wills, J.M.; Johansson, B. Experimental and theoretical identification of a new high-pressure phase of silica. *Nature* **1997**, *388*, 362–365. [[CrossRef](#)]
165. Ma, C.; Tschauer, O. A new high-pressure calcium aluminosilicate (CaAl₂Si_{3,5}O₁₁) in martian meteorites: Another after-life for plagioclase and connections to the CAS phase. In Proceedings of the 48th Lunar and Planetary Science Conference, The Woodlands, TX, USA, 20–24 March 2017; p. 1128.
166. Baziotis, I.P.; Yang, L.; Paul, S.; DeCarli, H.; Melosh, J.; McSween, H.Y.; Bodnar, R.J.; Taylor, L.A. The Tissint Martian meteorite as evidence for the largest impact excavation. *Nat. Commun.* **2013**, *4*, 1404. [[CrossRef](#)] [[PubMed](#)]
167. Walton, E.L.; Sharp, T.G.; Hu, J.; Filiberto, J. Heterogeneous mineral assemblages in Martian meteorite Tissint as a result of a recent small impact event on Mars. *Geochim. Cosmochim. Acta* **2014**, *140*, 334–348. [[CrossRef](#)]
168. Walton, E.L.; Spray, J.G. Mineralogy, microtexture, and composition of shock-induced melt pockets in the Los Angeles basaltic shergottite. *Meteorit. Planet. Sci.* **2003**, *38*, 1865–1875. [[CrossRef](#)]
169. He, Q.; Xiao, L.; Balta, J.B.; Baziotis, I.P.; Hsu, W.; Guan, Y. Petrography and geochemistry of the enriched basaltic shergottite Northwest Africa 2975. *Meteorit. Planet. Sci.* **2015**, *50*, 2024–2044. [[CrossRef](#)]
170. Boonsue, S.; Spray, J. Shock-induced phase transformations in melt pockets within Martian meteorite NWA 4468. *Spectrosc. Lett.* **2012**, *45*, 127–134. [[CrossRef](#)]

171. Ashworth, J.R.; Hutchison, R. Water in noncarbonaceous stony meteorites. *Nature* **1975**, *256*, 714–715. [[CrossRef](#)]
172. Treiman, A.H.; Barrett, R.A.; Gooding, J.L. Preterrestrial aqueous alteration of the Lafayette (SNC) meteorite. *Meteoritics* **1993**, *28*, 86–97. [[CrossRef](#)]
173. Treiman, A.H.; Lindstrom, D.J. Trace element geochemistry of Martian iddingsite in the Lafayette meteorite. *J. Geophys. Res.* **1997**, *102*, 9153–9163. [[CrossRef](#)]
174. Bridges, J.C.; Schwenzer, S.P. The nakhlite hydrothermal brine on Mars. *Earth Planet. Sci. Lett.* **2012**, *359–360*, 117–123. [[CrossRef](#)]
175. Tomkinson, T.; Lee, M.R.; Mark, D.F.; Smith, C.L. Sequestration of Martian CO₂ by mineral carbonation. *Nat. Commun.* **2013**, *4*, 2662. [[CrossRef](#)] [[PubMed](#)]
176. Gooding, J.L.; Wentworth, S.J.; Zolensky, M.E. Aqueous alteration of the Nakhla meteorite. *Meteoritics* **1991**, *26*, 135–143. [[CrossRef](#)]
177. Gillet, P.; Barrat, J.A.; Deloule, E.; Wadhwa, M.; Jambon, A.; Sautter, V.; Devouard, B.; Neuville, D.; Benzerara, K.; Lesourd, M. Aqueous alteration in the Northwest Africa 817 (NWA 817) Martian meteorite. *Earth Planet. Sci. Lett.* **2002**, *203*, 431–444. [[CrossRef](#)]
178. Day, J.M.D.; Taylor, L.A.; Floss, C.; McSween, H.Y. Petrology and chemistry of MIL 03346 and its significance in understanding the petrogenesis of nakhlites on Mars. *Meteorit. Planet. Sci.* **2006**, *41*, 581–606. [[CrossRef](#)]
179. Treiman, A.H.; Irving, A.J. Petrology of Martian meteorite Northwest Africa 998. *Meteorit. Planet. Sci.* **2008**, *43*, 829–854. [[CrossRef](#)]
180. Noguchi, T.; Nakamura, T.; Misawa, K.; Imae, N.; Aoki, T.; Toh, S. Laihunite and jarosite in the Yamato 00 nakhlites: Alteration products on Mars? *J. Geophys. Res.* **2009**, *114*, E10004. [[CrossRef](#)]
181. Thomas-Keprta, K.L.; Wentworth, S.J.; McKay, D.S.; Gibson, E.K. Field emission gun scanning electron (FEGSEM) and transmission electron (TEM) microscopy of phyllosilicates in Martian meteorites ALH 84001, Nakhla, and Shergotty. In Proceedings of the 31st Lunar and Planetary Science Conference, Houston, TX, USA, 13–17 March 2000.
182. Morris, R.V.; Klingelhofer, G.; Schroder, C.; Rodionov, D.S.; Yen, A.; Ming, D.W.; de Souza, P.A.; Fleischer, I.; Wdowiak, T.; Gellert, R.; et al. Mössbauer mineralogy of rock, soil, and dust at Gusev crater, Mars: Spirit's journey through weakly altered olivine basalt on the plains and pervasively altered basalt in the Columbia Hills. *J. Geophys. Res.* **2006**, *111*, E02S13. [[CrossRef](#)]
183. McLennan, S.M. Sedimentary silica on Mars. *Geology* **2003**, *31*, 315–318. [[CrossRef](#)]
184. Baker, L.L.; Agenbroad, D.J.; Wood, S.A. Experimental hydrothermal alteration of a Martian analog basalt: Implications for Martian meteorites. *Meteorit. Planet. Sci.* **2000**, *35*, 31–38. [[CrossRef](#)]
185. Tosca, N.J.; McLennan, S.M.; Lindsley, D.H.; Schoonen, M.A.A. Acid-sulfate weathering of synthetic Martian basalt: The acid fog model revisited. *J. Geophys. Res.* **2004**, *109*, E050003. [[CrossRef](#)]
186. Bandfield, J.L. High-silica deposits of an aqueous origin in western Hellas Basin, Mars. *Geophys. Res. Lett.* **2008**, *35*, 142–147. [[CrossRef](#)]
187. Mustard, J.F.; Murchie, S.L.; Pelkey, S.M.; Ehlmann, B.L.; Milliken, R.E.; Grant, J.A.; Bibring, J.-P.; Poulet, F.; Bishop, J.; Dobre, E.N.; et al. Hydrated silicate minerals on Mars observed by the Mars reconnaissance orbiter CRISM instrument. *Nature* **2008**, *454*, 305–309. [[CrossRef](#)] [[PubMed](#)]
188. Ehlmann, B.L.; Mustard, J.F.; Swayze, G.A.; Clark, R.N.; Bishop, J.L.; Poulet, F.; Des Marais, D.J.; Roach, L.H.; Milliken, R.E.; Wray, J.J.; et al. Identification of hydrated silicate minerals on Mars using MRO-CRISM: Geologic context near Nili Fossae and implications for aqueous alteration. *J. Geophys. Res.* **2009**, *114*, E00D08. [[CrossRef](#)]
189. Harvey, R.P.; Hamilton, V.E. Syrtis Major as the source region of the nakhlite/chassignite group of Martian meteorites: Implications for the geological history of Mars. In Proceedings of the Thirty-Sixth Lunar and Planetary Science Conference, League City, TX, USA, 14–18 March 2005.

